JEM Journal of Experimental Medicine

ARTICLE

STING agonist promotes CAR T cell trafficking and persistence in breast cancer

Nuo Xu[1,2], Douglas C. Palmer[3], Alexander C. Robeson[2], Peishun Shou[2], Hemamalini Bommiasamy[2], Sonia J. Laurie[2], Caryn Willis[2], Gianpietro Dotti[1,2], Benjamin G. Vincent[1,2,4,5,6], Nicholas P. Restifo[3], and Jonathan S. Serody[1,2,4,6]

CAR T therapy targeting solid tumors is restrained by limited infiltration and persistence of those cells in the tumor microenvironment (TME). Here, we developed approaches to enhance the activity of CAR T cells using an orthotopic model of locally advanced breast cancer. CAR T cells generated from Th/Tc17 cells given with the STING agonists DMXAA or cGAMP greatly enhanced tumor control, which was associated with enhanced CAR T cell persistence in the TME. Using single-cell RNA sequencing, we demonstrate that DMXAA promoted CAR T cell trafficking and persistence, supported by the generation of a chemokine milieu that promoted CAR T cell recruitment and modulation of the immunosuppressive TME through alterations in the balance of immune-stimulatory and suppressive myeloid cells. However, sustained tumor regression was accomplished only with the addition of anti–PD-1 and anti–GR-1 mAb to Th/Tc17 CAR T cell therapy given with STING agonists. This study provides new approaches to enhance adoptive T cell therapy in solid tumors.

Introduction

Chimeric antigen receptor (CAR) T cells have substantial activity against CD19-expressing B cell malignancies in humans (Neelapu et al., 2017; Maude et al., 2018). These receptors fuse the single-chain variable fragment (scFv) of an antibody specific to a tumor target with the signaling molecules of an effector T cell. This provides these cells with the specificity of an antibody and the effector function of T cells (Gorochov et al., 1992; Gross and Eshhar 1992).

Treatment of patients with solid tumors using CAR T cell therapy, however, has been less successful (Slaney et al., 2017; Tchou et al., 2017; Beatty et al., 2018). Potential barriers to CAR T cell efficacy against solid tumors include the suboptimal migration and persistence of CAR T cells in the tumor microenvironment (TME), impaired function mediated by the immunosuppressive TME, and CAR T cell exhaustion. Previous work from our group and others has shown that T helper 17 (Th17) and $CD8^+$ T 17 (Tc17) cells have enhanced persistence in solid tumors as compared with conventional Th1 cells (Boni et al., 2008; Paulos et al., 2010). Whether CAR T cells generated from Th/Tc17 cells are capable of persisting in the immunosuppressive TME of solid tumors remains unclear.

Development of an orthotopic immune-competent model to evaluate CAR T cell therapy

Given the need to understand mechanistically how to enhance CAR T cell function in solid tumors, we developed second- and third-generation murine CAR constructs targeting the proto-oncogene Neu (Fig. 1 A and Fig. S1 A). Second-generation CAR T cells were generated using the costimulatory domains from either CD28 (termed LH28z) or CD137 (4-1BB, termed LHBBZ). Third-generation CAR T cells were generated using both CD28 and CD137 signaling endodomains (LH28BBZ). Neu-specific CAR T cells were transduced and expanded with IL-7 and IL-15 (7/15 CAR T cells; Fig. 1 B and Fig. S1 B) at an equal ratio of $CD4^+$ to $CD8^+$ T cells (Fig. S1 C). These cells were functional in vitro, as they killed Neu-expressing target cells (Fig. 1 C and Fig. S1 D) and released proinflammatory cytokines only in response to Neu^+ tumor cells (Fig. 1 D). However, we consistently found that the transduction efficiency of the LHBBz construct was inferior to LH28z or LH28BBBz constructs (Fig. S1 B). Furthermore, both in vitro (Fig. S1 D) and in vivo (Fig. S1 E) experiments showed inferior antitumor activity of LH28BBz and LHBBz CAR T cells as compared with LH28z CAR T cells. Given these findings, we focused on enhancing the function of LH28z CAR T cells for the remainder of this work.

[1]Department of Microbiology and Immunology, University of North Carolina at Chapel Hill, Chapel Hill, NC; [2]Lineberger Comprehensive Cancer Center, University of North Carolina at Chapel Hill, Chapel Hill, NC; [3]Center for Cancer Research, National Cancer Institute, Bethesda, MD; [4]Department of Medicine, University of North Carolina at Chapel Hill, Chapel Hill, NC; [5]Curriculum in Bioinformatics and Computational Biology, University of North Carolina at Chapel Hill, Chapel Hill, NC; [6]Computational Medicine Program, University of North Carolina at Chapel Hill, Chapel Hill, NC.

Correspondence to Jonathan S. Serody: jonathan_serody@med.unc.edu; N.P. Restifo's present address is Lyell Immunopharma, San Francisco, CA.

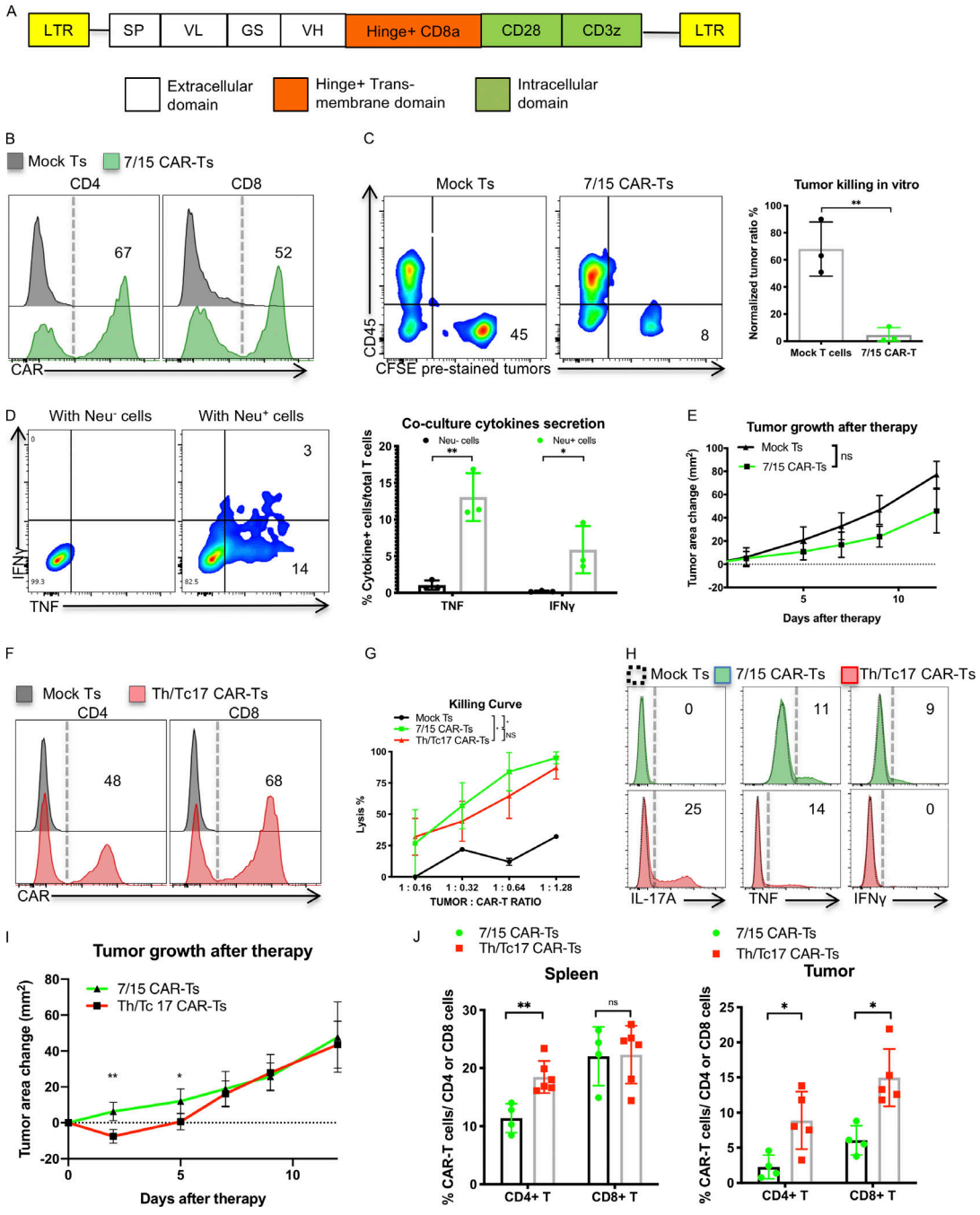

Figure 1. **Th/Tc17 CAR T cells exhibit enhanced early control of tumor growth over 7/15 CAR T cells owing to enhanced persistence in the tumor.** **(A)** Schematic of the LH28z CAR cassette encoding the scFv (7.16.4), hinge, and transmembrane domain from CD8, and intracellular domains from CD28 and CD3ζ. **(B)** Expression of CAR T receptor on transduced murine 7/15 CD4⁺ (left) and CD8⁺ (right) T cells. **(C)** Representative flow cytometry histograms depicting viability of Neu⁺ NT2 tumor cells in vitro after 3 d of coculture with 7/15 CAR T cells. Tumor cells were prelabeled with CFSE and plated before the addition of CAR T cells at a 1:1 ratio with tumor cells. **(D)** Intracellular staining illustrating IFN-γ and TNF production by 7/15 CAR T cells after coculture with Neu⁺ cells or Neu⁻ 3T3 cells at a 2:1 ratio. **(E)** Tumor area change (tumor area before therapy subtracted from area after therapy) was determined and compared in FVB-neu mice that received 7/15 CAR T cells or mock-transduced T cells (Mock Ts). **(F)** Expression of CAR T receptor on transduced Th17 (left) or Tc17 (right) cells. **(G)** In vitro killing of NT2 tumor cells by 7/15 CAR T and Th/Tc17 CAR T cells after overnight culture. **(H)** Histogram flow plots of IL-17A, TNF, and IFN-γ secretion by Th/Tc17 CAR T and 7/15 CAR T compared with mock T cells after coculture with Neu⁺ cells at 3:1 ratio for 6 h. **(I)** Tumor area change was calculated and compared in FVB-neu mice that received Th/Tc17 CAR T cells or 7/15 CAR T cells. **(J)** Detection of CD4⁺ and CD8⁺ CAR T cells in spleen or tumor by flow cytometry 5 d after injection of 7/15 CAR T cells or Th/Tc17 CAR T cells. Data are shown as mean ± SD; *, P < 0.05; **, P < 0.01; significance was determined by Student's *t* test or two-way ANOVA. *n* ≥ 5 mice per group with data from at least two independent experiments with the presented data pooled.

We evaluated the antitumor effects of CAR T cells in an orthotopic murine breast tumor model of locally advanced disease in immunocompetent mice (Fig. S1 F). Despite their in vitro cytolytic function, LH28z 7/15 CAR T cells were not able to control tumor growth in vivo (Fig. 1 E), even if hosts were lymphodepleted using irradiation before CAR T cell infusion (Fig. S1 G). Combining 7/15 LH28z CAR T cells with an anti–PD-1 mAb did not improve the outcome (Fig. S1 H) indicating that blocking the PD-1/PDL-1 pathway is insufficient for tumor control by 7/15 LH28z CAR T cells. Furthermore, very few CAR T cells were detected in the TME 5 d after treatment (Fig. S1 I), suggesting that the limited efficacy of 7/15 LH28z CAR T therapy was at least partly due to poor trafficking and persistence of CAR T cells in the TME.

Th/Tc17 CAR T cells have enhanced in vivo persistence

Th17 cells and their counterpart Tc17 cells ($CD8^+$ T cells that express IL-17A) have longer persistence in the TME, in part due to their better survival in vivo (Boni et al., 2008; Paulos et al., 2010). To evaluate if Th/Tc17 CAR T cells had better migration and/or persistence, we generated LH28z Th/Tc17 CAR T cells. We compared these cells with 7/15 CAR T cells. Transduction efficacy (Fig. 1 F) and killing activity in vitro (Fig. 1 G) were comparable. Th/Tc17 CAR T cells released IL-17A and TNF, while 7/15 CAR T cells expressed IFN-γ and TNF when cocultured with Neu^+ tumor cells in vitro (Fig. 1 H).

We next compared the in vivo antitumor effects of Th/Tc17 CAR T cells and 7/15 CAR T cells. Th/Tc17 CAR T cells were superior to 7/15 CAR T cells in controlling tumor growth up to day 5 after infusion (Fig. 1 I). To identify mechanisms associated with the improved early efficacy of Th/Tc17 CAR T cells, we isolated tumor-infiltrating lymphocytes from the TME and assessed their phenotype 5 d after therapy. There was a significant increase in both $CD4^+$ and $CD8^+$ CAR T cells in the tumor and $CD4^+$ CAR T cells in the spleen of mice receiving Th/Tc17 CAR T cells compared with the recipients of 7/15 CAR T cells (Fig. 1 J and Fig. S1 J). However, Th/Tc17 CAR T cells were only modestly increased in the TME, which may in part explain the lack of long-term tumor control. Thus, Th/Tc17 CAR T cells exhibit modestly improved migration/persistence to the TME and improved early tumor control, but this did not lead to a long-term antitumor response.

The stimulator of IFN genes (STING) agonist DMXAA greatly enhances CAR T efficacy

Given the short-term efficacy of Th/Tc17 CAR T cells in vivo, we sought an approach that would further enhance the migration and persistence of CAR T cells in the TME. Recent studies have shown a critical role for the STING pathway in generating "warm" tumors in the setting of checkpoint inhibitor therapy (Sen et al., 2019). Thus, we evaluated the activity of the STING agonist, DMXAA, in combination with CAR T cells. Mice were injected with NT2 tumors, and when tumors reached ∼50 mm^2, mice were given 7/15 or Th/Tc17 CAR T cells with DMXAA, which was given at a site remote from the tumor. Interestingly, DMXAA enhanced the persistence of 7/15 CAR T cells in the TME (Fig. 2 A). However, this was a modest increase in comparison to the increase when combined with Th/Tc17 CAR T cells. Thus, we focused on Th/Tc17 CAR T cells. The administration of DMXAA before Th/Tc17 CAR T cell infusion significantly improved antitumor efficacy (Fig. 2 B) and overall survival (Fig. 2 C) compared with mock-transduced T cells or Th/Tc17 CAR T cells alone.

We performed single-cell transcriptome sequencing (scRNA-seq) on $CD45^+$ cells isolated from the TME of mice that received Th/Tc17 CAR T with or without DMXAA. These evaluations were performed on day 7 after CAR T cell therapy, a time point at which we observed the greatest tumor control, and day 10, when tumors began to regrow (Fig. 2 D). Based on gene expression profiles, we identified three immune cell populations in the TME in mice receiving Th/Tc17 CAR T cells with or without DMXAA. Specifically, on day 7 after therapy, we identified clusters of T cells, macrophages, and a second myeloid cell cluster that each showed differential gene expression profiles in the presence or absence of DMXAA treatment (Fig. 2 E). In addition, we noted a relative increase in T cells and a relative decrease in regulatory T (T reg) cells and a subcluster of myeloid cells in the TME on day 7 after CAR T cell therapy (Fig. S2, A and B).

The most noticeable difference in the TME in mice receiving DMXAA was a substantial increase in T cells compared with animals given Th/Tc17 CAR T cells without DMXAA (Fig. 3 A and Fig. S2 A). $CD8^+$ T cells infiltrating the TME exhibited two different phenotypes. A subset expressed the transcription factor *rorc* and the cytokine *il17a* (Fig. 3, B and D), consistent with Tc17 cells. Interestingly, DMXAA treatment enhanced the accumulation of T cells that coexpressed the transcription factor *tbx21*, the proinflammatory cytokine *ifng*, the IFN-inducible chemokine receptor *cxcr3*, and *ccr5*, a trafficking receptor found on Th1/Tc1 cells (Fig. 3, B–D; and Fig. S2 C). This expression pattern is consistent with the presence of proinflammatory Tc1 cells converted from Tc17 cells in the presence of DMXAA. To confirm that the increase in T cells in mice receiving DMXAA was most likely due to the expansion of CAR T cells, flow cytometry was performed to detect CAR T cells in the TME. DMXAA treatment greatly increased the percentage and number of CAR T cells in the TME (Fig. 3 E). In addition, we found a strong association between the number of $CD8^+$ CAR T cells in the TME and tumor size in mice receiving DMXAA (Fig. 3 F). The flow cytometry data coupled with the presence of Th/Tc17 cells in the TME, which are not found in this model without Th/Tc17 CAR T cell infusion, strongly suggested that the T cells characterized in our single-cell analysis were CAR T cells. However, as we could not identify the CAR construct in all of the CAR T cells by single-cell analysis, we term these probable CAR T cells.

A combination of Tc17 and Th17 cells were necessary for antitumor efficacy using DMXAA, as Tc17 cells alone were not effective in tumor control (Fig. S2, D–F). To evaluate the effect of DMXAA on $CD4^+$ T cells, we performed scRNA-seq of $CD4^+$ T cells with or without DMXAA treatment (Fig. S2 G). Like the findings with $CD8^+$ T cells, there was an increase in probable CAR T cells expressing canonical genes for the Th17 phenotype (*rorc*) and genes for a cytolytic Th17/Th1 phenotype (*tbx21* and *irf4*). We also found an increase in the expression of *ifng* and chemokine receptor genes found on Th1 cells (*cxcr3* and *ccr5*; Fig.

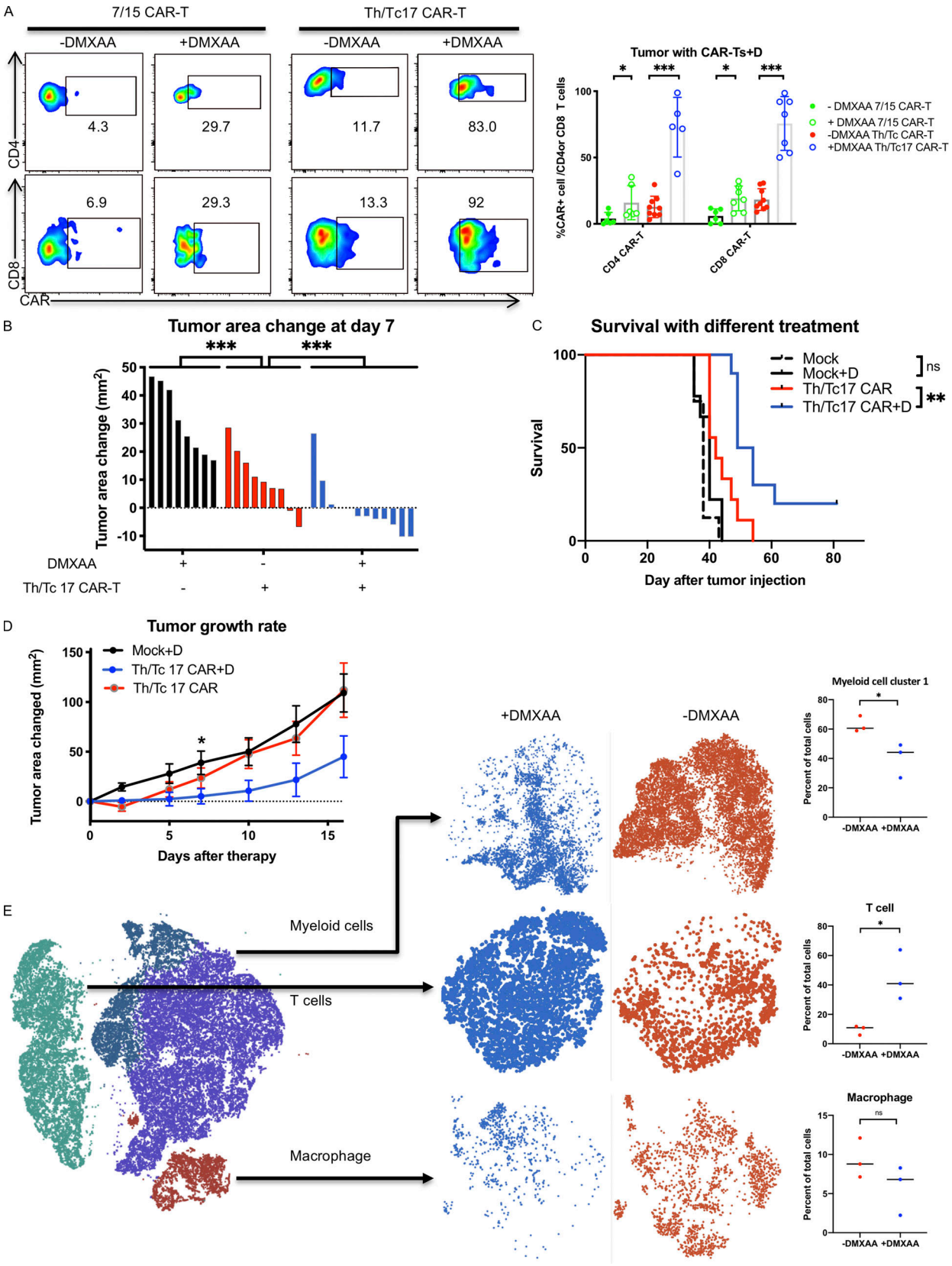

Figure 2. **Tumor control by Th/Tc17 CAR T cells is enhanced by DMXAA injection owing to altered composition of tumor infiltrating immune cells.** NT2 tumors were orthotopically injected into murine mammary pads. 21 d later, 500 µg of DMXAA was injected at a site distal to the tumor site, followed by injection of 3 × 10^6 mock T cells, 7/15 CAR T cells, or Th/Tc17 CAR T cells ($CD4^+$:$CD8^+$ at ∼1:1 ratio). **(A)** Representative flow cytometry histograms of CAR T detection in TME (left) and summary of accumulation of CAR T cells (right). **(B)** Change in tumor area was measured 7 d after treatment. **(C)** Kaplan–Meier

survival curve for the treatment cohorts. End point criteria for sacrifice was a tumor area of ≥200 mm^2. **(D)** Tumor area change 14 d after indicated therapy. **(E)** t-SNE analysis of pooled single-cell sequencing data generated from tumor-infiltrating $CD45^+$ immune cells 7 d after receiving Th/Tc17 CAR T cells in the presence or absence of DMXAA. Data were analyzed by unsupervised clustering, and populations were determined by expression of key markers, including *Cd3e* (T cells), *Adgre1* (macrophages), and *Itgam* and/or *Itgax* (myeloid cells). Right: Further classification of subpopulation between DMXAA-treated (+DMXAA) and non–DMXAA-treated (–DMXAA) mice and summary data comparing the frequency of indicated cell populations between +DMXAA and –DMXAA animals. Gating of flow cytometry data used fluorescence minus one controls for each individual experiment. Data are shown as mean ± SD; ns, not significant; *, $P < 0.05$; **, $P < 0.01$; ***, $P < 0.001$; significance was determined by Student's *t* test or log-rank Mantel–Cox test when comparing survival. $n \geq 5$ mice per group with data from at least two independent experiments (except for scRNA-seq), with the presented data pooled.

S2, H–K). We confirmed our single-cell data using flow cytometry, which demonstrated an increase in the number and percentage of $CD4^+$ CAR T cells in the presence of DMXAA (Fig. S2 L). This increase was associated with control of tumor growth (Fig. S2 M). To further validate our single-cell transcriptome data, we performed bulk quantitative PCR array evaluation of the TME. We found increased expression of genes associated with the Th1 and Th17 pathways in mice receiving Th/Tc17 CAR T cells and DMXAA treatment (Fig. S3, A and B). Finally, we demonstrated a critical role for IFN-γ expression by demonstrating the loss of activity of Th/Tc17 CAR T cell therapy plus DMXAA in mice that received anti–IFN-γ mAb (Fig. S3 C). Thus, DMXAA therapy was associated with a change in the phenotype of Th/Tc17 T cells to a proinflammatory dual Th17-Th1/Tc17-Tc1 phenotype, which is critical for tumor control.

CAR T cell exhaustion limits in vivo efficacy

LH28z Th/Tc17 CAR T cell therapy given with DMXAA controlled tumor growth for ∼10 d but did not eradicate the tumor. To investigate the cause of loss of activity of LH28z Th/Tc17 CAR T cells with DMXAA, we compared scRNA-seq of the TME on days 7 and 10 after CAR T cell therapy (Fig. S3 D). As early as day 7 after LH28z Tc/Th17 CAR T cell infusion, we found increased expression level of *pccd1* (PD-1), *lag3*, *cd160*, and *tox* by probable CAR T cells, with decreased expression of *tcf7* (Fig. 3, G–I; and Fig. S3, D and E). To confirm the single-cell data, flow analysis was performed on CAR T cells in the TME. There was a significant increase in PD-1–expressing $CD4^+$ and $CD8^+$ T cells on day 7 after Tc/Th17 LH28z CAR T cell treatment compared with mock-transduced CAR T cells (Fig. S3 F). We found increased expression of *S100A8* and *S100A9*, which together generate the protein calprotectin, which has been shown to induce T cell apoptosis (Ghavami et al., 2010; Wang et al., 2018; Fig. S3 G). Additionally, we found an increase in *cxcl2*, which has been associated with the recruitment of suppressive myeloid cells into the TME (Fig. 3 J). Overall, there were clear differences in the expression of specific exhaustion and or functional genes in T cells 7 or 10 d after DMXAA treatment.

Alteration of myeloid cells in the TME is associated with the function of DMXAA

DMXAA can modify the function of innate immune cells (Woo et al., 2014; Corrales et al., 2016). Thus, we evaluated the effects of the STING agonist on myeloid cells in the TME. Significant differences were found in the presence of M1-like and M2-like macrophages, inflammatory-like myeloid cells (iMCs), and myeloid-derived suppressive cells (MDSCs) in mice treated with and without DMXAA (Fig. 4, A and B; and Fig. S2 B). There was a marked decrease in the presence of M2-like macrophages expressing *retnla*, *mrc1*, *folr2*, and *il10* in the TME after treatment with DMXAA (Fig. 4 C and Fig. S4, A–C). This was associated with increased expression of genes associated with M1-like macrophages, including *nos2* and *inhba*. M1-like macrophages had increased expression of chemokines such as *cxcl9*, *cxcl10*, and *ccl5*, which recruit Th1/Tc1 T cells by binding to CXCR3- and CCR5-expressing cells (Fig. 4 D and Fig. S4, A–C). Consistent with the increased expression of *ifng* in the presence of DMXAA, macrophages had increased expression of *cd274* (PD-L1; Garcia-Diaz et al., 2017; Fig. S4 D). To demonstrate a critical role in the recruitment of CAR T cells to the TME by M1-like macrophages increased after DMXAA treatment, liposome clodronate was used to deplete these cells. M1-like macrophage depletion reversed the efficacy of DMXAA over the first week of Th/Tc17 CAR T cell therapy (Fig. 4 E).

A second cluster of myeloid cells was found after treatment with DMXAA with greatly enhanced expression of the transcription factor *batf2*, the chemokine ligands *cxcl10* and *ccl5*, and downstream genes related to inflammatory function (Kanemaru et al., 2017), including *socs1*, *nos2*, and *il12a* (Fig. 4, F–I; and Fig. S4, E–G). Additionally, there was reduced expression of *apoe*, *ptgs2* (Cox2), and *areg* and (Fig. S4, H–J) a gene expression profile consistent with MDSC-like cells. Thus, DMXAA was able to modulate the expression of genes associated with enhanced antitumor efficacy and to decrease the presence of protumorigenic myeloid cells.

To characterize the TME immediately before tumor growth, we evaluated myeloid cell subsets on day 10 after Th/Tc17 CAR T cell infusion with DMXAA. As shown in Fig. 4 (J–M), there was a significant change in the TME over this 4-d period, with a marked increase in the presence of MDSC-like cells expressing *ptgs2*, *areg*, and *apoe* (Fig. S4, J and K). There was a significant decrease in the presence of *batf2*-expressing myeloid cells (Fig. 4, L and M). Thus, the diminished function of LH28z Th/Tc17 CAR T cells plus DMXAA was strongly associated with the reestablishment of an immunosuppressive TME.

Targeting CAR T cell exhaustion and immature myeloid cells enhanced CAR efficacy

Given our data regarding the expression of PD-1 on CAR T cells and the marked changes in the immunosuppressive nature of the TME, we evaluated whether targeting these pathways could enhance the long-term efficacy of LH28z Th/Tc17 CAR T cells plus DMXAA. To this end, we treated mice with LH28z Th/Tc17 CAR T cells plus DMXAA along with anti–PD-1 and anti–GR-1 mAb therapy (Fig. 5 A). This approach led to significantly improved overall survival and control of tumor growth compared with

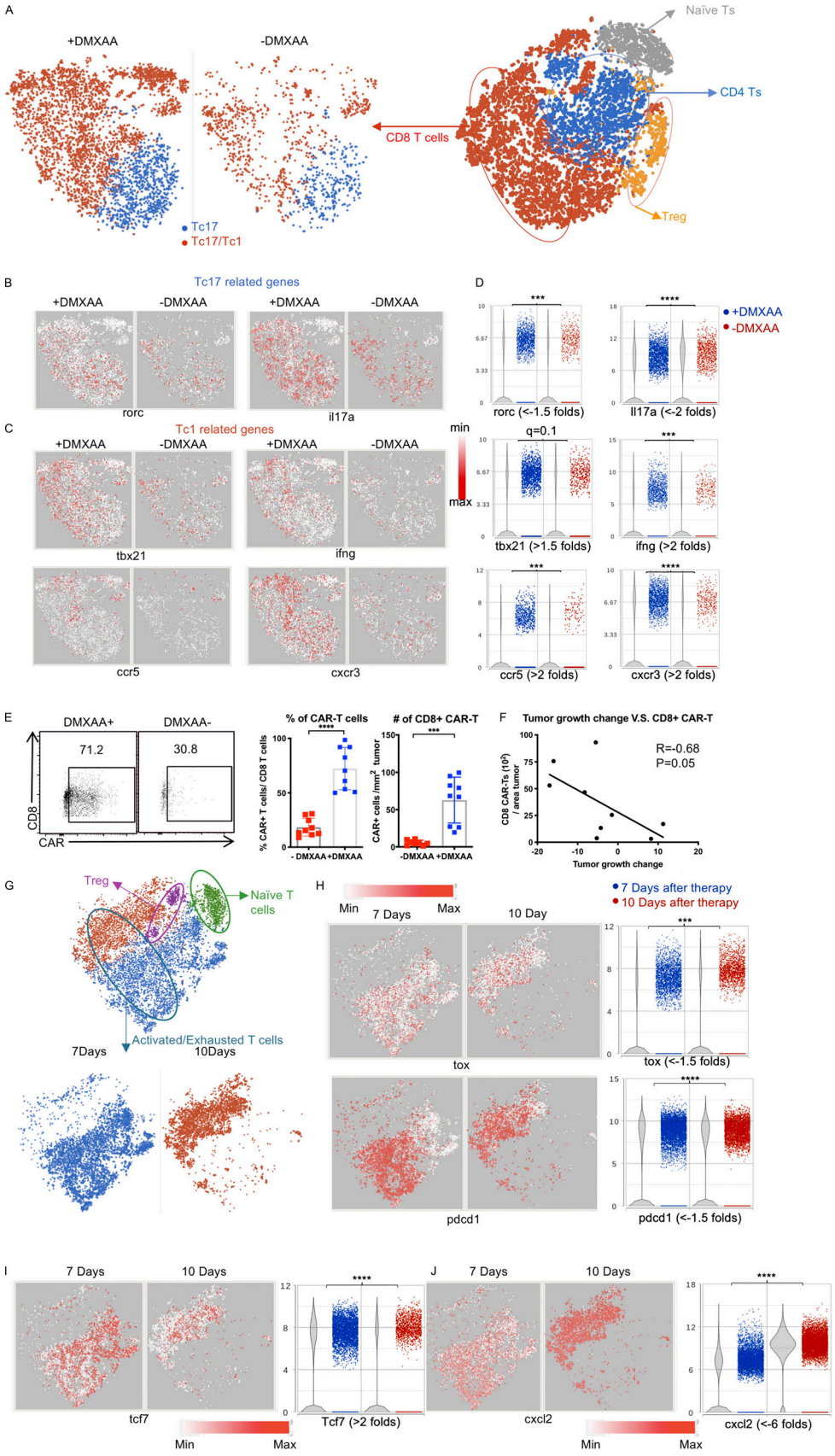

Figure 3. **DMXAA treatment enhances the number and cytotoxicity of Tc17 CAR T cells in the TME, although they eventually become exhausted.** **(A)** T cell populations were subdivided based on expression of *Cd8* and *Cd44* (activated CD8 T cells), *Cd44* (naive T cells), and *Cd4* and *Foxp3* (T reg cells). CD8$^+$ T cells were compared between the +DMXAA and −DMXAA treatment groups, and each subpopulation was examined further as described below. **(B)** t-SNE

plots of CD8⁺ T cells for Tc17-related genes. **(C)** t-SNE plots of CD8⁺ T cells for Tc1-related genes. **(D)** Violin plots depicting the distribution and change in expression of genes identified in B and C. **(E)** Validation of single-cell sequencing data using flow cytometry to detect CD8⁺ CAR T cells. Representative flow plots (left) and frequency (middle) and number (right) of CD8⁺ CAR T cells. **(F)** Analysis of the correlation between tumor growth and absolute cell number of CAR-expressing CD8⁺ T cells/cm² tumor. **(G)** Activated or exhausted T cells were selected by unsupervised clustering result of tumor-infiltrating immune cells from 7 and 10 d after Th/Tc17 CAR+DMXAA therapy and shown as a t-SNE plot. **(H)** t-SNE plot (left) and violin plot (right) of T cells assessing genes associated with T cell exhaustion. **(I)** t-SNE plot (left) and violin plot (right) of T cells for genes associated with T cell effector function. **(J)** t-SNE plot (left) and violin plot (right) of T cells for genes associated with chemokine secretion. Data (excluding scRNA-seq) represent one of two independent experiments ($n \geq 5$ mice per group). Single-cell sequencing data represent two to three mice/treatment group, and statistical significance was determined by differential GSA from Partek flow workstation. *, $q < 0.05$; **, $q < 0.01$; ***, $q < 0.001$; ****, $q < 0.0001$ in the change of gene expression level. Fold change is +DMXAA versus −DMXAA or 7 versus 10 d. For percentage/number change, please refer to Fig. S2 C. Flow-cytometric analysis was pooled from two independent experiments and is shown as mean ± SD. Statistical analysis for cytometric analysis was determined by Student's *t* test; ***, $P < 0.001$; ****, $P < 0.0001$.

mice that received CAR T cell therapy with DMXAA and either anti–PD-1 or anti–GR-1 mAb therapy (Fig. 5, B–D). However, substantial antitumor activity was found only in mice that received CAR T cells plus DMXAA with either anti–PD-1 or anti–GR-1 mAb therapy (Fig. 5, B and C). There was no antitumor activity in mice that did not receive CAR T cells or DMXAA (Fig. 5, B and C). Importantly, optimal tumor control required CAR T cell therapy with DMXAA and anti–PD-1 and anti–GR-1 mAbs (Fig. 5 D).

To evaluate whether combination therapy with DMXAA and anti–PD-1 and anti–GR-1 mAbs could also enhance the antitumor activity of 7/15 CAR T cells, we compared tumor growth in mice receiving anti–GR-1 and anti–PD-1 mAb with DMXAA and given either 7/15 or Th/Tc17 CAR T cells. Much greater antitumor activity was found with the administration of Th/Tc17 CAR T cells compared with 7/15 CAR T cells when combined with DMXAA and anti–PD-1 and anti–GR-1 mAbs (Fig. S5, A and B). Even in the absence of anti–PD-1 and anti–GR-1 therapy, there was an increase in CAR T cells in the TME (Fig. 2 A), compared with the spleen (Fig. S5 C) in mice receiving Th/Tc17 CAR T cells compared with 7/15 CAR T cells. There was much greater proliferation of CD4⁺ CAR T cells in mice receiving Th/Tc17 compared with 7/15 CAR T cells (Fig. S5 D). For CD8⁺ CAR T cells, we found a significant increase in the number of CD8⁺ central memory CAR T cells from day 7 to day 12 after infusion in the TME of mice receiving Th/Tc17 compared with 7/15 CAR T cells, which were predominantly effector memory T cells on day 7 (Fig. S5, E and F). Differences in the number of effector versus central memory CAR T cells were supported by the increased number of Th/Tc17 CAR T cells with a precursor effector phenotype (CD127⁺ and KLRG1⁻; Fig. S5 G). In conclusion, sustained tumor regression caused by Th/Tc17 CAR T cells was associated with enhanced proliferation and expansion of central memory T cells.

The human STING agonist cGAMP enhances Th/Tc17 CAR T cell efficacy

Previous studies have shown that DMXAA does not bind to human STING and thus does not activate the human protein. To test the effect of a clinically relevant STING agonist in potentiating the antitumor efficacy of Th/Tc17 CAR T cells, we used 2,3-cGAMP (cGAMP), a STING agonist that binds to both human and murine STING. cGAMP was given subcutaneously in a manner similar to DMXAA in combination with Th/Tc17 CAR T cells. The administration of cGAMP enhanced the proliferation and infiltration of Th/Tc17 CAR T cells at the tumor site (Fig. 6 A). This was associated with a significant decrease in tumor growth (Fig. 6, B and C) and enhanced survival of mice receiving Th/Tc17 CAR T cells (Fig. 6 D). While the overall survival was not significantly different, mice treated with cGAMP and Th/Tc17 CAR T cells had better tumor control >21 d after therapy compared with mice receiving DMXAA and Th/Tc17 CAR T cells (Fig. 6, C and D). Thus, a clinically relevant STING agonist, cGAMP, enhanced the function of Th/Tc17 CAR T cells in this model.

Efficacy associated with cytokine release–like syndrome

Treatment of mice with Th/Tc17 CAR T cells, DMXAA, and anti–PD-1 and anti–GR-1 mAbs led to significant tumor control, with the majority of mice tumor-free 30 d after treatment. However, we found that most of the mice that received this therapy, including critically the anti–GR-1 mAb to deplete immunosuppressive myeloid cells, exhibited significant weight loss and hunching consistent with a cytokine release–like syndrome (Fig. 7 A). This was correlated with increased mortality in these mice (Fig. 7 B). Treatment efficacy correlated with the development of this syndrome (Fig. 7 C). This toxicity was observed in mice receiving either DMXAA or cGAMP as the STING agonist (Fig. 7, A and B). To determine a cause for the increased toxicity in these mice, we evaluated cytokine levels from the serum of mice receiving Th/Tc17 CAR with DMXAA and anti–PD-1 ± anti–GR-1 mAb treatment. Significant increases in CCL2, G-CSF, and IL-6 were found in mice given anti–GR-1 mAb compared with mice that did not receive anti–GR-1 treatment (Fig. 7 D). Mice receiving Th/Tc17 CAR T cells with DMXAA and anti–PD-1 and anti–GR-1 mAbs were then treated with an anti–IL-6 antibody, which has demonstrated efficacy in the treatment of cytokine release syndrome (CRS) in human subjects receiving CAR T cells (Giavridis et al., 2018; Li et al., 2019). Mice were given anti–IL-6 antibody on day 5 at the onset of weight loss in animals treated with combination therapy (Fig. 7 B). As shown in Fig. 7 (E and F), treatment with anti–IL-6 mAb was associated with improved survival in mice receiving combination therapy and did not abrogate the antitumor efficacy of combination therapy (Fig. 7 G).

Discussion

Although CAR T cells targeting CD19 have been successful in treating patients with B cell malignancies (Neelapu et al., 2017;

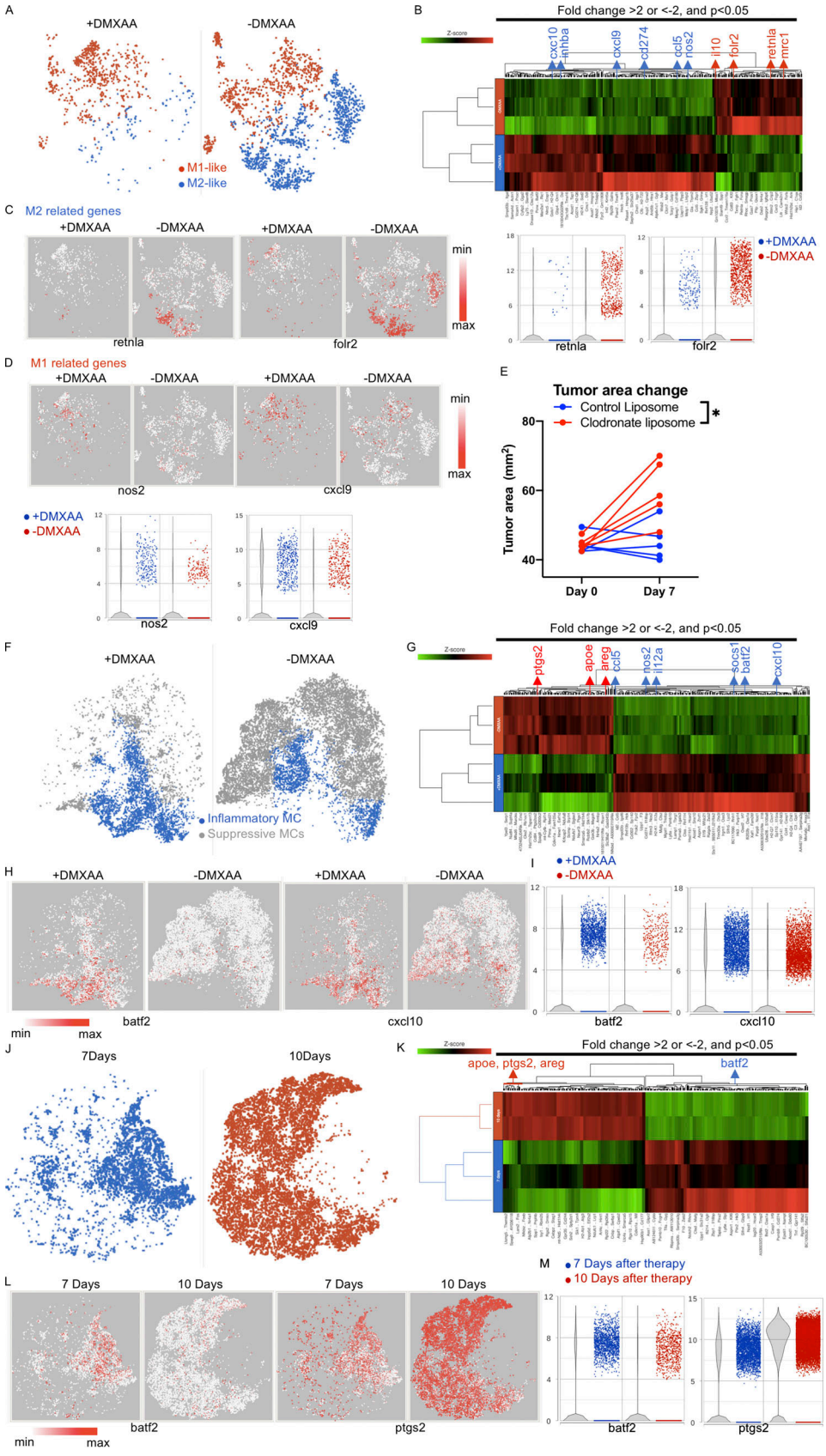

Figure 4. **DMXAA reduces the accumulation of suppressive macrophages and enhances the trafficking of T cells in the TME, but this effect is eventually lost due to the return of immunosuppressive cells. (A)** t-SNE plot of macrophage populations identified by unsupervised clustering (Fig. 2), selected and classified as M1- or M2-like, and compared between mice receiving therapy with or without DMXAA treatment. **(B)** Heatmap of genes identified in

A exhibiting a greater than twofold change in expression following DMXAA treatment, with a significant difference of P < 0.05 (determined by GSA). **(C)** t-SNE plot (left) and violin plots (right) showing expression of M2-related genes. **(D)** t-SNE plot (left) and violin plots (right) showing expression of M1-related genes. **(E)** Tumor area before and after 7 d of treatment with Th/Tc17 CAR T and DMXAA therapy after injection of clodronate or control liposomes. **(F)** t-SNE plot of myeloid populations identified by unsupervised clustering (Fig. 2), selected and classified as inflammatory myeloid cells or suppressive myeloid cells, and compared between mice in the presence or absence of DMXAA treatment. **(G)** Heatmap of genes identified in F exhibiting a greater than twofold change in expression following DMXAA treatment, with a significant difference of P < 0.05 (determined by GSA). **(H)** t-SNE plot depicting genes preferentially expressed in inflammatory myeloid cells. **(I)** Violin plots showing distribution and change in expression of genes highlighted in H. Myeloid cells from unsupervised clustering 7 and 10 d after therapy were selected. **(J)** t-SNE plot of myeloid cells between 7 and 10 d after therapy. **(K)** Heatmap of proinflammatory or suppressive genes that exhibited a greater than twofold change in expression following DMXAA treatment, with a significant difference of P < 0.05. **(L)** t-SNE plot of myeloid cells illustrating genes associated with the inflammatory and suppressive functions of myeloid cells. **(M)** Violin plots showing distribution and change of indicated gene expression in L. *, P < 0.05; significance was determined by Student's *t* test. Single-cell sequencing data represent two to three mice/treatment group. Macrophage depletion assay was done independently twice with representative result shown.

Maude et al., 2018), the clinical activity of CAR T cells in patients or animal models with solid tumors has been modest (Slaney et al., 2017; Tchou et al., 2017; Beatty et al., 2018). Using a rational and sequential approach, we have implemented a combinatorial immunotherapy strategy based on CAR T cells polarized to a Th/Tc17 phenotype, anti–PD-1 mAb, STING agonists DMXAA or c-GAMP, and anti–GR-1 mAb that leads to tumor eradication in an immunocompetent syngeneic model of breast cancer. The most compelling finding was the ability of the STING agonists, DMXAA and c-GAMP, given at a site remote of the tumor, to promote CAR T cell recruitment and persistence at the tumor site. To our knowledge, these data are the first to demonstrate the function of a STING agonist in altering the trafficking properties of adoptive T cellular products. Furthermore, this activity did not require intratumoral injection of the STING agonist.

A critical aspect of effective CAR T cell therapy is the ability of the transferred cells to traffic to tumor sites. CAR T cells expanded ex vivo and infused intravenously in patients home physiologically to secondary lymphoid organs such as the bone marrow and lymph nodes, which explains in part the robust antitumor effects of CAR T cells observed in patients with leukemia, lymphoma, and multiple myeloma (Hunter et al., 2016). In contrast, T cells do not constitutively traffic to breast tissue. Th/Tc17 cells have enhanced biodistribution to peripheral tissues as compared with Th1 cells, and this may explain in part our observation that Th/Th17 CAR T cells showed superior persistence in the tumor compared with IL7/15 CAR T cells (Fig. 2 A and Fig. S1 J). To further increase CAR T cell accumulation in solid tumors, engineering processes have been exploited using tumor-associated chemokine gradients or by modifying the stiffness of the extracellular matrix (Moon et al., 2011; Caruana et al., 2015; Adachi et al., 2018). Here, we report that the STING agonists DMXAA and cGAMP promoted CAR T cell persistence within the TME. DMXAA treatment led to increased expression of *cxcl9* and *cxcl10* by myeloid cells within the TME. These chemokines recruit CXCR3-expressing Th/Tc1 T cells. Correlating with this finding, DMXAA treatment was associated with a marked increase in the number of CAR T cells through day 10 after therapy. Interestingly, these T cells had an altered phenotype, as they did not generate IFN-γ before infusion but expressed *ifng*, *tbx21*, and *cxcr3* after therapy with DMXAA. T cells expressing IL-17A and IFN-γ have been found in other models to induce significant tissue pathology (Buonocore et al., 2010; Hirota et al., 2011). Our data using anti–IFN-γ, which led to a complete loss of the activity of these CAR T cells in vivo, would support a critical role for the conversion of Th/Tc17 CAR T cells to a Th/Tc1 phenotype in their antitumor activity in vivo.

The immunocompetent mouse model we developed allowed us to assess how the myeloid cell compartment affected the antitumor activity of CAR T cells. We demonstrate that the persistence of Th/Tc17 CAR T cells in the TME was associated with enhanced expression of genes associated with M1-like macrophages and a marked loss of genes associated with M2-like macrophages and MDSC-like cells. The decrease in *batf2*-expressing iMCs was associated with the inability of CAR T cells to control tumor growth. Thus, these data suggest that enhancing CAR T cell trafficking and persistence without altering the immunosuppressive TME is unlikely to lead to significant sustained antitumor effects in solid tumors (Newick et al., 2017; De La Rochere et al., 2018).

Th/Tc17 CAR T cell persistence within the TME, which is promoted by the proinflammatory myeloid switch caused by a STING agonist, does not prevent exhaustion of CAR T cells, which requires checkpoint blockade to sustain CAR T cell–mediated tumor control. Moreover, a rapid influx of immunosuppressive monocytic MDSCs within the TME was also observed and associated with diminished control of tumor growth. Previous work had shown that CAR T cells specific for CEA were inhibited by liver myeloid-derived suppressor cells when given via the portal vein to mice with liver metastasis (Burga et al., 2015). Here, we found that depletion of MDSC-like cells, using anti–GR-1 mAb in combination with CAR T cells, STING agonist, and PD-1 blockade, allowed sustained regression of the tumor. We observed, however, that the optimal combination also led to the development of rapid cachexia consistent with a CRS. Recent work has highlighted the critical role of myeloid cells in the pathogenesis of CRS (Norelli et al., 2018; Staedtke et al., 2018; Sterner et al., 2019). Our data suggest that MDSCs, and perhaps other immunosuppressive myeloid cells, limit the antitumor efficacy of CAR T cells but also attenuate the severity of the inflammatory reaction. Fully licensing CAR T cells by depleting MDSCs exacerbated a CRS, which responded to IL-6 blockade, as observed in patients receiving CAR T cells targeting CD19.

In summary (Fig. 8), we have found that suboptimal trafficking and persistence/expansion of CAR T cells greatly limits their antitumor activity in an orthotopic model of locally advanced breast cancer. The STING agonists, DMXAA or cGAMP,

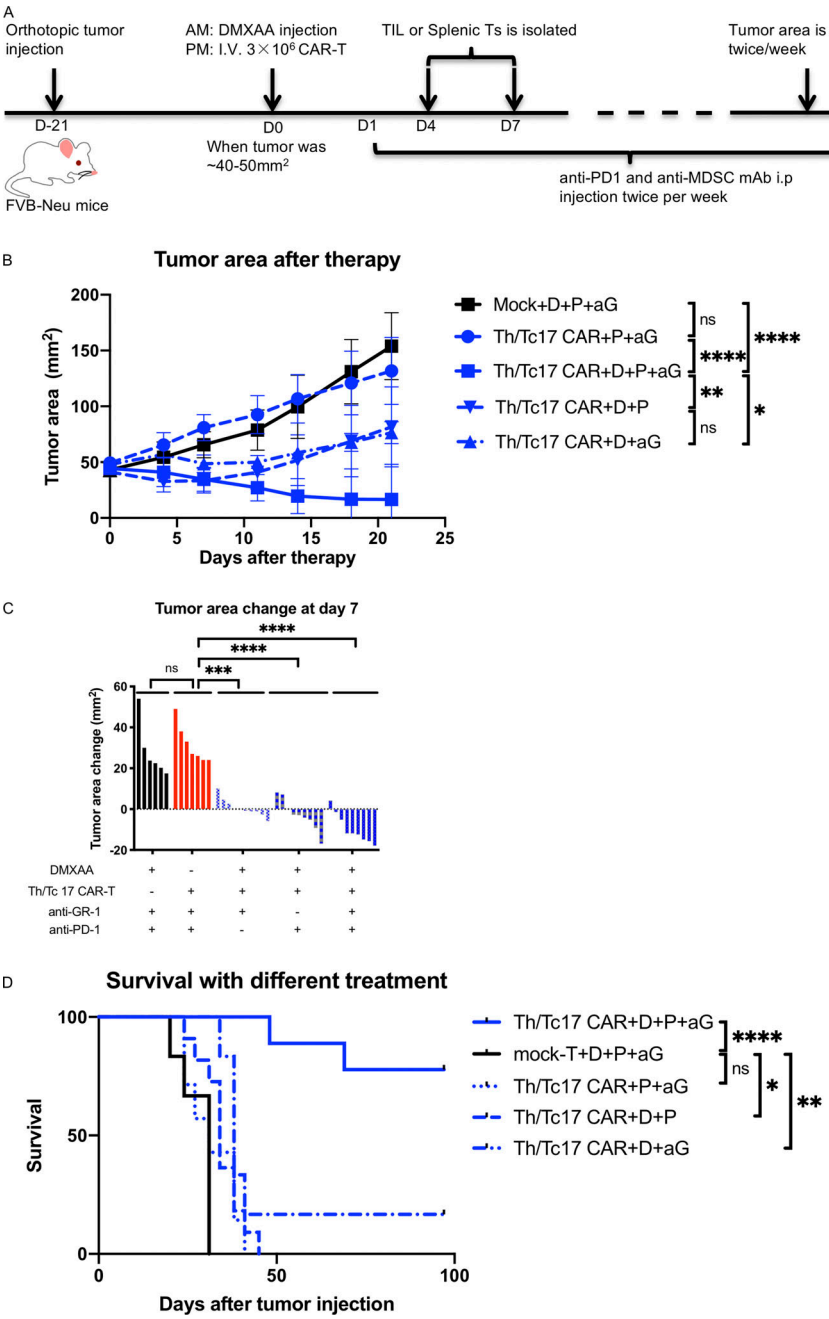

Figure 5. **DMXAA is required for tumor remission after Th/Tc17 CAR T, DMXAA, anti–PD-1, and anti-Gr1 treatment.** Animals received injections of anti–PD-1 (200 µg/mouse) and anti-Gr1 (300 µg/mouse) twice weekly, beginning a day after CAR T injection in additional to therapy described in Fig. 2 (Th/Tc17 CAR + D + aP + aG). **(A)** Schematic describing therapy schedule. **(B)** Summary of tumor growth (in area) in the first 3 wk after CAR T therapy. **(C)** Change in tumor area was assessed 7 d after administration of Th/Tc CAR + triple therapy or in the absence of DMXAA, anti–PD-1, anti–Gr-1, or CAR T cells (mock T cells to model the absence of CAR T cells). **(D)** Kaplan–Meier survival curve indicating mortality over 100 d for the four treatment groups. Data are shown as mean ± SD; ns, not significant; *, P < 0.05; **, P < 0.01; ***, P < 0.001; ****, P < 0.0001; significance was determined by Student's *t* test or two-way ANOVA when comparing tumor growth change between groups or log-rank Mantel–Cox test when comparing survival. *n* ≥ 5 mice per group with the data from at least two independent experiments, with the presented data pooled.

greatly enhanced the trafficking and persistence of Th/Tc17 CAR T cells. These data suggest a viable strategy for boosting CAR T activity in solid tumors, as cGAMP is in clinical trials for the treatment of patients with cancer (Woo et al., 2014), there are multiple ongoing clinical trials using approaches to inhibit MDSCs for patients with malignant disease (Fleming et al., 2018), and some clinical trials are currently evaluating the combination of CAR T cells with checkpoint blockade.

Materials and methods

Tumor cell culture

The 3T3 cell line was obtained from ATCC and cultured in DMEM (Gibco) supplemented with 10% FBS (Gemini) and 1% penicillin/streptomycin (Pen/Strep; Invitrogen). 3T3-Neu and NT2 tumors have been described (Reilly et al., 2000). 3T3-Neu cultures were made as described and cultured with the addition of 0.3 µM methotrexate. NT2 cells (passage 6) were cultured in RPMI-1640 (Gibco) supplemented with 20% FBS, 2 mM L-glutamine (Invitrogen), 12 mM Hepes (Invitrogen), 0.1 mM nonessential amino acid (Invitrogen), 1 mM sodium pyruvate (Invitrogen), 1% Pen/Strep, 50 µM 2-mercaptoethanol (Invitrogen), and 0.2 U/ml Novolin R-insulin (Novo Nordisk). The virus encoding the LH28z CAR was cultured in PLAT-E cells from Cell Biolabs in DMEM supplemented with 10% FBS and 1% Pen/Strep. All cells used for the generation of the CAR constructs were used within three passages in vitro, and 0.05% trypsin (Invitrogen) was used for digestion between passages.

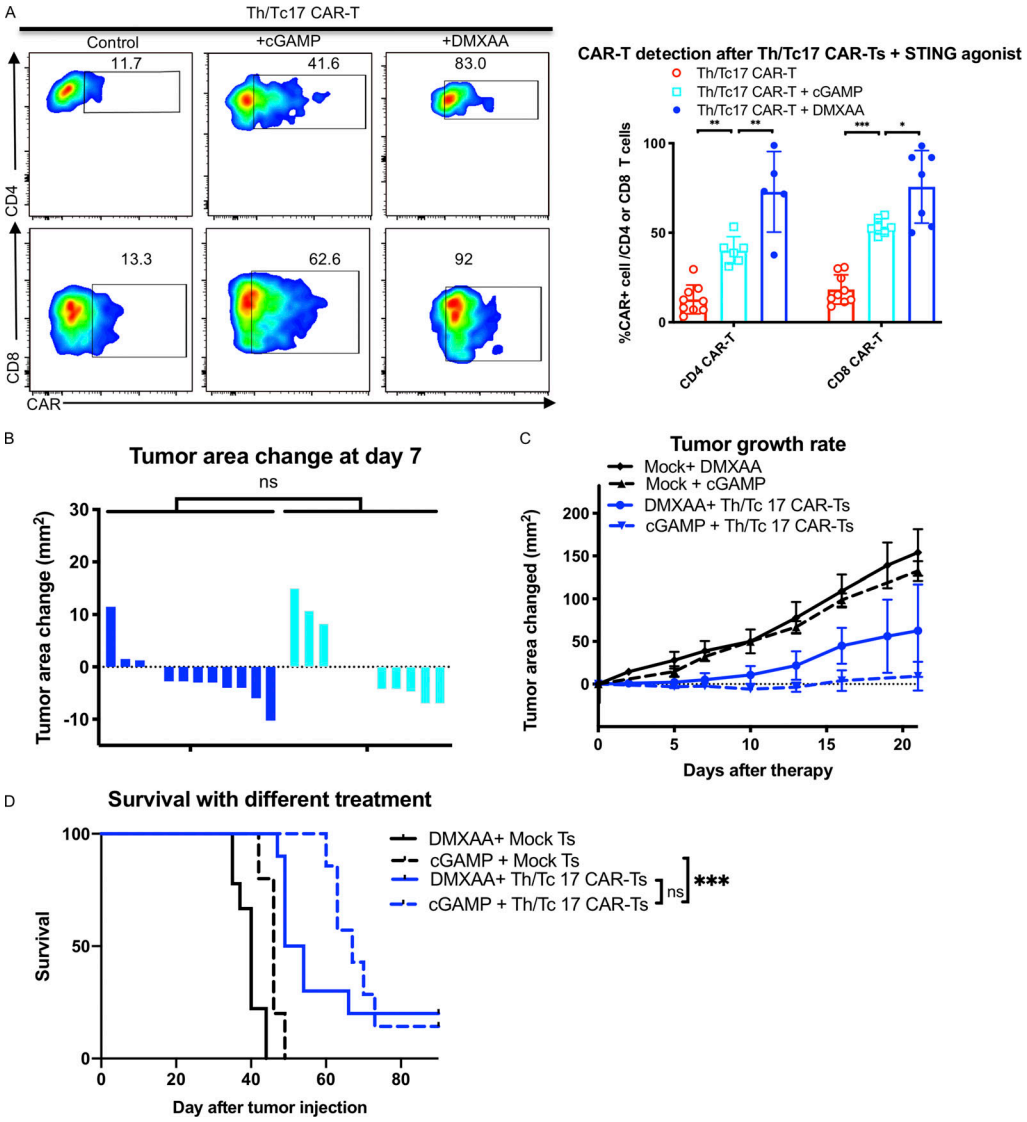

Figure 6. **Tumor control by Th/Tc17 CAR T cells is enhanced by human STING agonist 2,3-cGAMP**. NT2 tumors were orthotopically injected into murine mammary pads. 21 d later, 25 µg of cGAMP was injected at a site distal to the tumor site, followed by injection of 3 × 10^6 mock T cells, 7/15 CAR T cells, or Th/Tc17 CAR T cells ($CD4^+$:$CD8^+$ at ∼1:1 ratio). **(A)** Representative flow cytometry histograms of CAR T cells detection at in the TME (left) and summary of accumulation of CAR T cells (right). **(B)** Change in tumor area measured over 7 d after treatment. **(C)** Tumor area change 21 d after indicated therapy. **(D)** Kaplan–Meier survival curve for the treatment cohorts. Endpoint criteria for sacrifice was tumor area of ≥200 mm^2. Gating of flow cytometry data used fluorescence minus one controls for each individual experiment. Data are shown as mean ± SD; ns, not significant; *, P < 0.05; **, P < 0.01; ***, P < 0.001; significance was determined by Student's *t* test or log-rank Mantel–Cox test when comparing survival. *n* ≥ 5 mice per group with the data from at least two independent experiments, with the presented data pooled.

Vector construct

7/15 and Th/Tc17 CARs contain the scFv of LH28z construct generated from the 7.16.4 antibody. Whole RNA from the 7.16.4 hybridoma was isolated (RNEasy Kit; Qiagen) and made into cDNA (M-MLV Reverse Transcription kit; Invitrogen). Antibody heavy and light chains were cloned with IgH or IgL primer mix (iRepertoire) and sequenced by Sanger sequencing (Genewiz). CAR cDNAs were cloned into a construct containing murine CD8 transmembrane domain and intracellular domain from murine CD28 or 4-1BB and CD3ξ (LH28z and LHBBz). The CAR construct was then cloned into MSGV plasmid driven by 5′ LTR. The plasmid construct has been described (Chinnasamy et al., 2010).

Viral construct preparation and transduction

Plasmids encoding CAR (LH28z) and pCL-Eco retrovirus packaging vector (Novus) were cotransfected into PLAT-E cells using Lipofectamine 2000 (Invitrogen). The supernatant from LH28z-transfected PLAT-E cells was collected after 48 h and stored at −80°C. For T cell transduction, LH28z, LHBBz, or LH28z/LHBBz virus was plated onto a retronectin-coated plate (Takara) and incubated at 32°C for 2 h, followed by the addition of activated T cells. The coculture was spun at 1,200 *g* for 90 min and stored at 37°C overnight.

T cell activation and culture

For 7/15 CAR T cells, splenocytes from 8–14-wk-old female FVB/NJ mice (Jackson Laboratory) were harvested and activated

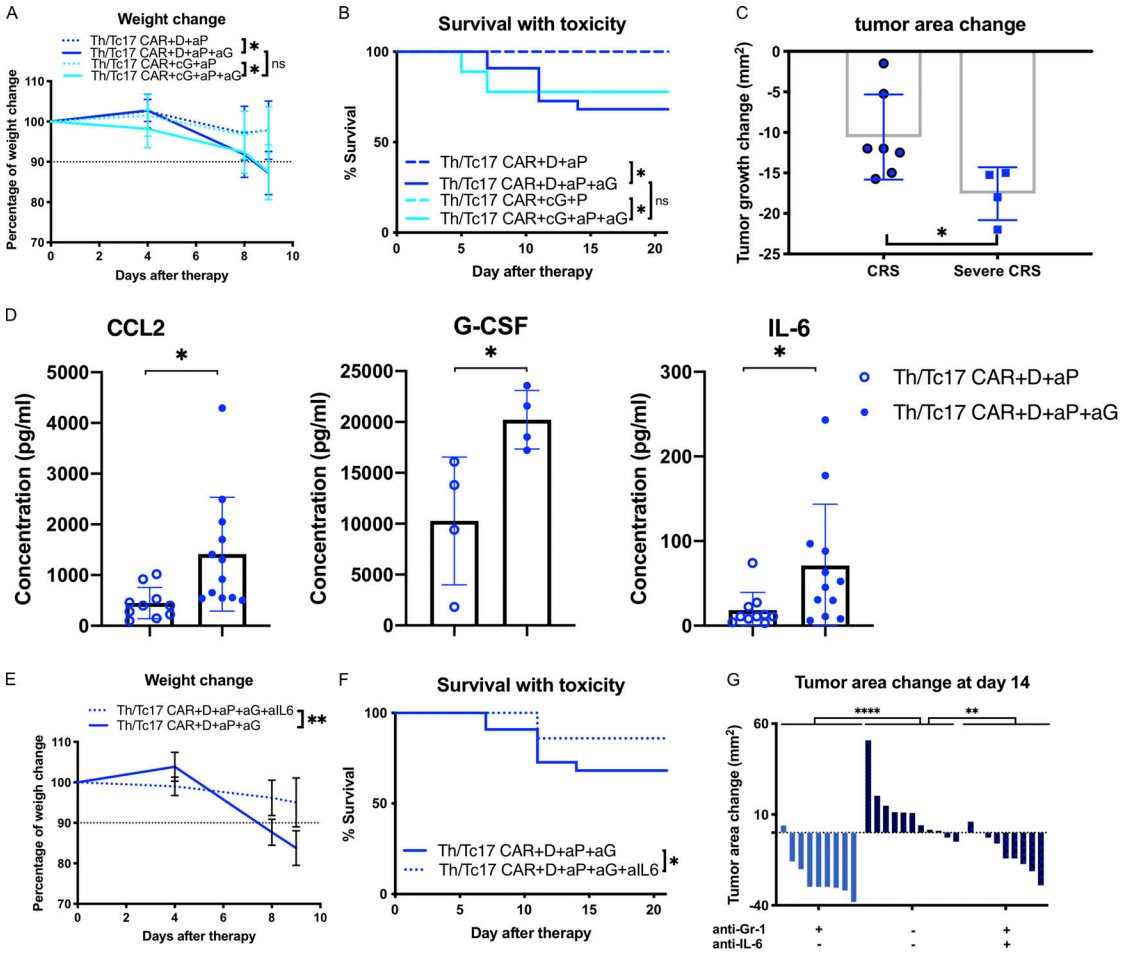

Figure 7. **Depletion of myeloid cells with anti-Gr1 during Th/Tc17 CAR + D/cG + aP regimen leads to cytokine release-like syndrome.** Mice received Th/Tc17 CAR + D + P with or without twice-weekly anti–Gr-1 injections after CAR T therapy. **(A)** Quantification of weight loss as percentage of total change in body weight following Th/Tc17 CAR + D/cG + P or Th/Tc17 CAR + D/cG + aP + aG. **(B)** Kaplan–Meier survival curve indicating mortality over 20 d in the presence or absence of anti–Gr-1 treatment. **(C)** Change in tumor area 7 d after Th/Tc17 CAR + D + P or Th/Tc17 CAR + D + aP + aG treatment in mice that survived but lost >10% of their initial weight (CRS-like) compared with mice that eventually died from CRS-like symptoms (severe CRS-like). **(D)** Serum cytokine levels of CCL2, mG-CSF, and IL-6 measured 5 d after therapy. **(E)** Quantification of weight loss as percentage of total change in body weight following Th/Tc17 CAR + D + aP + aG + aIL-6 or Th/Tc17 CAR + D + aP + aG treatment. **(F)** Kaplan–Meier survival curve indicating mortality over 20 d in the presence or absence of anti–IL-6 mAb treatment. **(G)** Tumor growth change at 14 d after the therapy in the presence or absence of anti–Gr-1 and/or anti–IL-6 mAb. Data are shown as mean ± SD; ns, not significant; *, $P < 0.05$; **, $P < 0.01$; ****, $P < 0.0001$; significance was determined by Student's *t* test and log-rank Mantel–Cox test when comparing survival. $n \geq 5$ mice per group with the data from at least two independent experiments with the presented data pooled.

using plate-bound anti-CD3 (145-2C11; Invitrogen) and anti-CD28 mAb (37.51; Invitrogen) and cultured in RPMI-1640 supplemented with 10% FBS, 2 mM L-glutamine, 12 mM Hepes, 0.1 mM nonessential amino acid, 1 mM sodium pyruvate, 1% Pen/Strep, 50 µM 2-mercaptoethanol, along with the addition of 1 µg/ml IL-7 and IL-15 (Peprotech). 48 h later, T cells were transduced with retrovirus and cultured for an additional 3 d with IL-7 and IL-15. For Th/Tc17 CAR T cells, naive $CD4^+$ and $CD8^+$ T cells were isolated from the spleens of 8–14-wk-old female FVB/NJ mice (Jackson Laboratory) using murine naive CD4/CD8 T Cell Isolation Kit (Miltenyi) according to the manufacturer's instructions. T cells were activated using plate-bound anti-CD3 and anti-CD28 mAb (Invitrogen). For the first week, the culture was maintained as described above with the addition of TGF-β1 (2 ng/ml), IL-1β (10 ng/ml), TNF (20 ng/ml), IL-6 (30 ng/ml; Peprotech), anti–IFN-γ (R4-6A2, 10 µg/ml; Bio X Cell), and anti–IL-2 (JES6-5H4, 10 µg/ml; Bio X Cell; Th17 cytokine cocktail). 2 d after activation, T cells were transduced with retrovirus and kept in culture with Th17 cytokine cocktail for the rest of the week. During the second week, cultured T cells were reactivated using plate-bound anti-CD3 and anti-CD28 mAb and maintained in Th17 cytokine cocktail plus IL-23 (15 ng/ml; Peprotech).

Murine tumor model

8–12-wk-old female FVB-Neu mice (FVB/N-Tg(MMTVneu) from Jackson Laboratory were used under a protocol approved by University of North Carolina Institutional Animal Care and Use Committee. For tumor inoculation, mice were intradermally injected with 5×10^4 NT2 tumor cells into an axillary mammary gland. 21 d later (day 0), 1.5×10^6 $CD4^+$ and 1.5×10^6 $CD8^+$ CAR T cells were injected intravenously. Tumors were measured

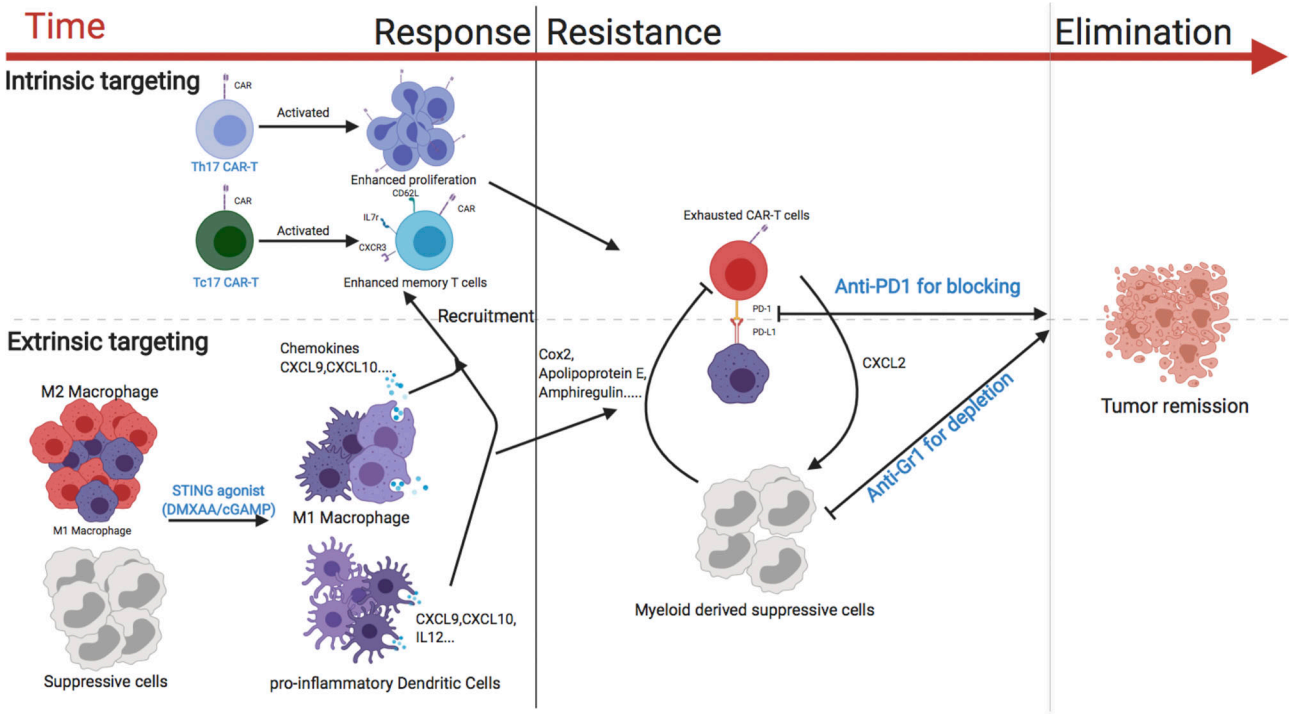

Figure 8. **Model of the activity of CAR T cells against breast cancer.** The use of Th/Tc17 CAR T cells with enhanced proliferation and memory status (intrinsic modification) along with DMXAA/cGAMP to enhance trafficking and reduce immunosuppression in the TME (extrinsic modification) is critical for the effective antitumor response of CAR T cells against breast cancer (left). CAR T exhaustion (intrinsic resistance) and reversion back to an immunosuppressive TME state (extrinsic resistance) are associated with loss of CAR T cell function (middle). The addition of anti–PD-1 to overcome exhaustion (intrinsic modification) and the depletion of suppressive myeloid cells with anti–Gr-1 (extrinsic modification) leads to sustained tumor remission (right).

twice weekly with calipers, and the tumor area was calculated as length × width. The change of tumor area was determined by subtracting the tumor area before CAR T injection from the value on the day of measurement. Per institutional guidelines, tumor-bearing mice were sacrificed when the tumor area reached 200 mm^2 or lost >20% of total body weight. For tumor-bearing animals receiving combination therapy, animals underwent lymphodepletion with 5 Gy of whole-body irradiation (X-RAD 320; Precision X-Ray) 1 d before CAR T injection. On the morning of day 0, mice were injected with 500 µg of DMXAA (Tocris) or 25 µg of 2,3-cGAMP (InvivoGen) distal to the site of tumor growth, with CAR T cells injected in the afternoon. Starting 1 d after CAR T infusion, anti–PD-1 (J43; Bio X Cell; 200 µg/mouse), anti–Gr-1 (RB6-8C5; Bio X Cell; 300 µg/mouse), or anti–IFN-γ (R4-6A2; Bio X Cell; 250 µg/mouse) mAb were injected i.p. into recipients. For anti–IL-6 treatment, anti–IL-6 (MP5-20F3; Bio X Cell; 200 µg/mouse first dose and 100 µg/mouse subsesquent doses) was injected i.p. starting 5 d after therapy and for the next 4 d.

In vivo tumor-infiltrating immune cell isolation

At indicated time points, tumors were bluntly resected, cut into small pieces, and processed into a single-cell suspension using gentleMACS Dissociator (Miltenyi). Lymphocyte enrichment was achieved by isolating cells at the interface of 44% Percoll (Sigma-Aldrich) in medium and Lympholyte-M (Cedarlane). Isolated immune cells were stained as described below. The lymphocyte fraction was not enriched in experiments in which absolute cell number was determined.

In vivo tumor-infiltrating immune cells isolation for scRNA-seq analysis

At day 7 or day 10 after CAR T therapy, tumors were bluntly resected and cut into small pieces and digested using Tumor Dissociation Kit, mouse (Miltenyi), in gentleMACS Dissociator (Miltenyi) according to the manufacturer's instruction. After digestion, dead and dying cells were magnetically separated using a Dead Cell Removal Kit (Miltenyi), after which immune cells were magnetically enriched using CD45 (TIL) MicroBeads (Miltenyi). Single cells were partitioned using a Chromium Controller (10x Genomics), and gene expression sequencing libraries were generated using Chromium Single Cell 3′ Library & Gel Bead Kit v3 (10x Genomics). The libraries were pooled and sequenced using an Illumina NovaSeq 6000 (Illumina). Raw base call files were demultiplexed with Cell Ranger 3.1.0 (10x Genomics) and bcl2fastq Conversion Software v2.20.0 (Illumina). The output result was for analysis using Partek flow workstation. Detailed information for single-cell sequencing is given in Table 1.

scRNA-seq result analysis

Single-cell results from the Cell Ranger output were analyzed using Partek flow workstation as follows. Single-cell results from each sample of Cell Ranger output was filtered using a

Table 1. **Details regarding tumor single-cell sequencing analysis**

DMXAA treatment	Tumor area (mm^2)	Total $CD45^+$ cells	Cells for scRNA-seq	Cells recovered for analysis
7 d				
+	38.5	550,000	16,000	6,959
+	45	425,000	16,000	9,842
+	33.75	225,000	16,000	3,989
–	59.5	162,500	16,000	11,842
–	55.25	212,500	16,000	8,541
–	63	175,000	16,000	8,246
10 d				
+	45	195,000	16,000	8,044
+	41.25	195,000	16,000	11,786

single-cell quality assurance/quality control filter to exclude doublets/multiplets, cells expressing <30 genes per cell, and dead cells. Processed results were normalized using the recommended methods, including log normalization of gene expression and scaling to count per million. Results were filtered out by feature (gene) not expressed in 99% of samples. Replicate samples were pooled and clustered with an unsupervised method based on principle component analysis, using the first 16 principle components. Clustered plots were visualized by t-distributed stochastic neighbor embedding (t-SNE) plot, in which cells were clustered using shared nearest neighbor. Populations were determined by expression of key markers, including *Cd3e* (T cells), *Adgre1* (macrophages), and *Itgam* and/or *Itgax* (myeloid cells), and T cells were further clustered by expression of *Cd8* and *Cd44* (activated CD8 T cells), lack of *Cd44* (naive T cells), *Cd4* and *Cd44* (activated CD4 T cells), and *Cd4* and *Foxp3* (T reg cells). For comparison, samples from each treatment group were pooled by mean expression to simulate bulk RNA-seq and compared using gene-specific analysis (GSA) directly. Gene hits that reached $P < 0.05$ with more than 2-fold or less than −2-fold expression difference were reported and shown as a heatmap for pooled samples (macrophages and myeloid cells) or $q < 0.05$ with 2- or −2-fold expression difference for nonpooled samples (T cells). Further detailed analysis steps can be found on the Partek flow page (https://documentation.partek.com/pages/viewpage.action?pageId=12943422); parameter settings were default unless indicated.

Flow cytometry

Anti-Neu CAR T cells were detected using recombinant Neu/Her2.Fc fusion protein conjugated with PE (Neu-PE; Creative Biomart). Antibodies used in in vitro assays included anti–CD45-FITC/e450 (30-F11; Invitrogen), anti–IFN-γ-APC (XMG1.2; Invitrogen), anti–TNF-PE-Cy7 (MP6-XT22; Invitrogen), and anti–IL-17A-PE (eBio17B7; Invitrogen). Tumor-infiltrating immune cells were detected and analyzed with anti–CD45-FITC, anti–CD3-e450 (17A2; Invitrogen), anti–CD4-BV510 (GK1.5; BioLegend), anti–CD8-APC-Cy7 (53-6.7; BD Biosciences), anti–CD44-PerCP5.5 (IM7; Invitrogen), anti–CD62L-APC (MEL-14; Invitrogen), anti–CD11b-BV711 (M1/70; Invitrogen), anti–F4/80-BV605 (BM8; Invitrogen), anti–Gr-1-Percp5.5 (RB6-8C5; Invitrogen), anti–PD-1-PE-Cy7 (J43; Invitrogen), anti–CD127-BV421 (A7R34; BioLegend), and anti–KLGR1-BV605 (2F1; BD Biosciences). For in vivo intracellular protein staining, anti–Foxp3-PerCP5.5 (FJK-16S; Invitrogen) and anti–Ki67-APC (SOLA15; Invitrogen) were used. Dead cells were excluded with Fixable Viability Stain 700 (BD Biosciences), and Fc receptors were blocked with Fc block (BD Biosciences). Cell number was determined using Count Bright Beads (Invitrogen). Data were collected using a BD LSR-Fortessa or BD Canto cytometer (BD Biosciences). Data were analyzed with FlowJo software (TreeStar).

Flow cytometry–based T cell cytolytic assay

For coculture killing assays, 10^6 NT2 tumor cells were labeled with 5 µM CFSE (Invitrogen) and plated in culture medium for 24 h. CAR T, mock-transfected T cells, or no T cells were added the next day at the indicated ratios and cocultured in T cell medium without cytokines for 3 d. Supernatant and trypsinized cells were collected and stained with 7-amino-actinomycin D (BD Biosciences) and anti-CD45 (30-F11; Invitrogen). Killing was measured by flow cytometry after gating on $CFSE^+$, 7-amino-actinomycin D–negative, and $CD45^-$ tumor cells and normalized to groups without T cell addition. For the killing curve, NT2 tumor cells were labeled with CFSE and plated at 10^5 cells/well in a 48-well plate. CAR T cells, mock T cells, or no T cells at the indicated ratios were added 12 h later. Cocultures were maintained in T cell medium without cytokines for 18 h, and cell killing was measured as described above. Percentage tumor lysis was calculated by subtracting the number of live tumor cells from 100% and dividing by the total number of live tumor cells in the group with no T cells added.

Cytokine release assay

5×10^5 3T3 or 3T3-Neu cells were treated with trypsin and processed into a single-cell suspension before culture with CAR T or mock T cells at the indicated ratios in T cell medium without additional cytokine. 5 µg/ml of brefeldin A (BD Biosciences) was added after the first hour of coculture. Cells were stimulated for 5 h and then pelleted for extracellular staining with anti-CD45,

followed by fixation and permeabilization using Fix/Perm Kit (BD Biosciences) according to the manufacturer's instructions. Anti–IFN-γ, anti-TNF, and anti–IL-17A were used for intracellular cytokine staining and detected by flow cytometry.

Cytokine measurements

Cell culture supernatants or serum were collected by direct collection or cardiovascular puncture and stored at −20°C before use. The level of cytokines was determined by ELISA or magnetic Luminex assay according to the manufacturer's instructions (R&D Systems). Data were collected using the Lumina-200 System and analyzed with Bio-Plex Manager 6.1 software (Bio-Rad).

Real-time PCR array

Whole-tumor RNA was isolated using the RNEasy Kit (Qiagen) and reverse transcribed using RT^2 First Strand Kit (Qiagen). Quantitative RT-PCR was performed according to the manufacturer's instructions with the RT^2 Profiler PCR Array Mouse Th17 Response (PAMM-073ZE-4; Qiagen) and performed on the QuantStudio 6K (Applied Biosystems). Count threshold values were determined with ABI software, and data analysis was performed using the web-based RT2 Profiler PCR Array Data Analysis v3.5 (Qiagen). Fold-change was normalized to a housekeeping gene (*Gusb*).

Online supplemental material

Fig. S1 describes the generation and efficacy of the CAR construct with different intracellular signaling motifs and an enhanced in vivo tumor growth control efficacy by Th/Tc17 CAR T cells compared with 7/15 CAR T cells. Fig. S2 describes scRNA-seq results in percentages and the gene expression change of CD4$^+$ T cells in the TME from scRNA-seq. Fig. S3 describes the change of gene expression in the TME 7 d after DMXAA treatment by RNA microarray and T cells 10 d after DMXAA treatment by scRNA-seq. Fig. S4 describes the scRNA-seq result on macrophages and myeloid cells on days 7 and 10 after DMXAA treatment. Fig. S5 reports the in vivo efficacy of 7/15 CAR T cells after DMXAA, anti-Gr1, and anti–PD-1 therapy and compares it with Th/Tc17 CAR T cell treatment.

Acknowledgments

We acknowledge Mark Ross from the University of North Carolina (UNC) Lineberger Animal Studies Core Facility for animal treatment service. We also gratefully acknowledge UNC High Throughput Sequencing Facility for their sequencing service.

This work was supported by grants from the National Cancer Institute (P50 CA058223) and the University Cancer Research Fund. The UNC Lineberger Animal Studies Core is supported in part by a National Cancer Institute Center Core Support Grant (CA16086) to the UNC Lineberger Comprehensive Cancer Center.

Author contributions: N. Xu designed and performed experiments, analyzed data, and wrote the manuscript. D.C. Palmer and N. Xu built the CAR construct. A.C. Robeson and N. Xu performed the scRNA-seq. P. Shou, H. Bommiasamy, and N. Xu performed the CRS study. C. Willis assisted in the analysis of scRNA-seq data. P. Shou, S.J. Laurie, G. Dotti, B.G. Vincent, N.P. Restifo, and J.S. Serody provided suggestions on experimental design, data analysis, and manuscript writing. J.S. Serody conceived the project and wrote and edited the manuscript.

Disclosures: N. Xu reported a patent to STING on CAR T therapy against solid tumor pending. A.C. Robeson reported personal fees from Precision BioSciences, Inc. outside the submitted work. B.G. Vincent reported "other" from GeneCentric Therapeutics outside the submitted work. N.P. Restifo reported a patent to UNC/NCI pending. J.S. Serody reported grants from Merck Inc. and Glaxo Smith Kline outside the submitted work; in addition, J.S. had a patent for the use of STING agonist to enhance CAR T cell function pending. No other disclosures were reported.

Submitted: 29 April 2020
Revised: 22 September 2020
Accepted: 12 November 2020

References

Adachi, K., Y. Kano, T. Nagai, N. Okuyama, Y. Sakoda, and K. Tamada. 2018. IL-7 and CCL19 expression in CAR-T cells improves immune cell infiltration and CAR-T cell survival in the tumor. *Nat. Biotechnol.* 36: 346–351. https://doi.org/10.1038/nbt.4086

Beatty, G.L., M.H. O'Hara, S.F. Lacey, D.A. Torigian, F. Nazimuddin, F. Chen, I.M. Kulikovskaya, M.C. Soulen, M. McGarvey, A.M. Nelson, et al. 2018. Activity of mesothelin-specific chimeric antigen receptor T cells against pancreatic carcinoma metastases in a phase 1 trial. *Gastroenterology.* 155: 29–32. https://doi.org/10.1053/j.gastro.2018.03.029

Boni, A., P. Muranski, L. Cassard, C. Wrzesinski, C.M. Paulos, D.C. Palmer, L. Gattinoni, C.S. Hinrichs, C.C. Chan, S.A. Rosenberg, and N.P. Restifo. 2008. Adoptive transfer of allogeneic tumor-specific T cells mediates effective regression of large tumors across major histocompatibility barriers. *Blood.* 112:4746–4754. https://doi.org/10.1182/blood-2008-07-169797

Buonocore, S., P.P. Ahern, H.H. Uhlig, I.I. Ivanov, D.R. Littman, K.J. Maloy, and F. Powrie. 2010. Innate lymphoid cells drive interleukin-23-dependent innate intestinal pathology. *Nature.* 464:1371–1375. https://doi.org/10.1038/nature08949

Burga, R.A., M. Thorn, G.R. Point, P. Guha, C.T. Nguyen, L.A. Licata, R.P. DeMatteo, A. Ayala, N. Joseph Espat, R.P. Junghans, and S.C. Katz. 2015. Liver myeloid-derived suppressor cells expand in response to liver metastases in mice and inhibit the anti-tumor efficacy of anti-CEA CAR-T. *Cancer Immunol. Immunother.* 64:817–829. https://doi.org/10.1007/s00262-015-1692-6

Caruana, I., B. Savoldo, V. Hoyos, G. Weber, H. Liu, E.S. Kim, M.M. Ittmann, D. Marchetti, and G. Dotti. 2015. Heparanase promotes tumor infiltration and antitumor activity of CAR-redirected T lymphocytes. *Nat. Med.* 21:524–529. https://doi.org/10.1038/nm.3833

Chinnasamy, D., Z. Yu, M.R. Theoret, Y. Zhao, R.K. Shrimali, R.A. Morgan, S.A. Feldman, N.P. Restifo, and S.A. Rosenberg. 2010. Gene therapy using genetically modified lymphocytes targeting VEGFR-2 inhibits the growth of vascularized syngenic tumors in mice. *J. Clin. Invest.* 120: 3953–3968. https://doi.org/10.1172/JCI43490

Corrales, L., S.M. McWhirter, T.W. Dubensky Jr., and T.F. Gajewski. 2016. The host STING pathway at the interface of cancer and immunity. *J. Clin. Invest.* 126:2404–2411. https://doi.org/10.1172/JCI86892

De La Rochere, P., S. Guil-Luna, D. Decaudin, G. Azar, S.S. Sidhu, and E. Piaggio. 2018. Humanized mice for the study of immuno-oncology. *Trends Immunol.* 39:748–763. https://doi.org/10.1016/j.it.2018.07.001

Fleming, V., X. Hu, R. Weber, V. Nagibin, C. Groth, P. Altevogt, J. Utikal, and V. Umansky. 2018. Targeting myeloid-derived suppressor cells to bypass tumor-induced immunosuppression. *Front. Immunol.* 9:398. https://doi.org/10.3389/fimmu.2018.00398

Garcia-Diaz, A., D.S. Shin, B.H. Moreno, J. Saco, H. Escuin-Ordinas, G.A. Rodriguez, J.M. Zaretsky, L. Sun, W. Hugo, X. Wang, et al. 2017. Interferon receptor signaling pathways regulating PD-L1 and PD-L2 expression. *Cell Rep.* 19:1189–1201. https://doi.org/10.1016/j.celrep.2017.04.031

Ghavami, S., M. Eshragi, S.R. Ande, W.J. Chazin, T. Klonisch, A.J. Halayko, K.D. McNeill, M. Hashemi, C. Kerkhoff, and M. Los. 2010. S100A8/A9 induces autophagy and apoptosis via ROS-mediated cross-talk between mitochondria and lysosomes that involves BNIP3. *Cell Res.* 20:314–331. https://doi.org/10.1038/cr.2009.129

Giavridis, T., S.J.C. van der Stegen, J. Eyquem, M. Hamieh, A. Piersigilli, and M. Sadelain. 2018. CAR T cell-induced cytokine release syndrome is mediated by macrophages and abated by IL-1 blockade. *Nat. Med.* 24:731–738. https://doi.org/10.1038/s41591-018-0041-7

Gorochov, G., J. Lustgarten, T. Waks, G. Gross, and Z. Eshhar. 1992. Functional assembly of chimeric T-cell receptor chains. *Int. J. Cancer Suppl.* 7:53–57.

Gross, G., and Z. Eshhar. 1992. Endowing T cells with antibody specificity using chimeric T cell receptors. *FASEB J.* 6:3370–3378. https://doi.org/10.1096/fasebj.6.15.1464371

Hirota, K., J.H. Duarte, M. Veldhoen, E. Hornsby, Y. Li, D.J. Cua, H. Ahlfors, C. Wilhelm, M. Tolaini, U. Menzel, et al. 2011. Fate mapping of IL-17-producing T cells in inflammatory responses. *Nat. Immunol.* 12:255–263. https://doi.org/10.1038/ni.1993

Hunter, M.C., A. Teijeira, and C. Halin. 2016. T cell trafficking through lymphatic vessels. *Front. Immunol.* 7:613. https://doi.org/10.3389/fimmu.2016.00613

Kanemaru, H., F. Yamane, K. Fukushima, T. Matsuki, T. Kawasaki, I. Ebina, K. Kuniyoshi, H. Tanaka, K. Maruyama, K. Maeda, et al. 2017. Antitumor effect of *Batf2* through IL-12 p40 up-regulation in tumor-associated macrophages. *Proc. Natl. Acad. Sci. USA.* 114:E7331–E7340. https://doi.org/10.1073/pnas.1708598114

Li, J., R. Piskol, R. Ybarra, Y.J. Chen, J. Li, D. Slaga, M. Hristopoulos, R. Clark, Z. Modrusan, K. Totpal, et al. 2019. CD3 bispecific antibody-induced cytokine release is dispensable for cytotoxic T cell activity. *Sci. Transl. Med.* 11:eaax8861. https://doi.org/10.1126/scitranslmed.aax8861

Maude, S.L., T.W. Laetsch, J. Buechner, S. Rives, M. Boyer, H. Bittencourt, P. Bader, M.R. Verneris, H.E. Stefanski, G.D. Myers, et al. 2018. Tisagenlecleucel in children and young adults with B-cell lymphoblastic leukemia. *N. Engl. J. Med.* 378:439–448. https://doi.org/10.1056/NEJMoa1709866

Moon, E.K., C. Carpenito, J. Sun, L.C. Wang, V. Kapoor, J. Predina, D.J. Powell Jr., J.L. Riley, C.H. June, and S.M. Albelda. 2011. Expression of a functional CCR2 receptor enhances tumor localization and tumor eradication by retargeted human T cells expressing a mesothelin-specific chimeric antibody receptor. *Clin. Cancer Res.* 17:4719–4730. https://doi.org/10.1158/1078-0432.CCR-11-0351

Neelapu, S.S., F.L. Locke, N.L. Bartlett, L.J. Lekakis, D.B. Miklos, C.A. Jacobson, I. Braunschweig, O.O. Oluwole, T. Siddiqi, Y. Lin, et al. 2017. Axicabtagene ciloleucel CAR T-cell therapy in refractory large B-cell lymphoma. *N. Engl. J. Med.* 377:2531–2544. https://doi.org/10.1056/NEJMoa1707447

Newick, K., S. O'Brien, E. Moon, and S.M. Albelda. 2017. CAR T cell therapy for solid tumors. *Annu. Rev. Med.* 68:139–152. https://doi.org/10.1146/annurev-med-062315-120245

Norelli, M., B. Camisa, G. Barbiera, L. Falcone, A. Purevdorj, M. Genua, F. Sanvito, M. Ponzoni, C. Doglioni, P. Cristofori, et al. 2018. Monocyte-derived IL-1 and IL-6 are differentially required for cytokine-release syndrome and neurotoxicity due to CAR T cells. *Nat. Med.* 24:739–748. https://doi.org/10.1038/s41591-018-0036-4

Paulos, C.M., C. Carpenito, G. Plesa, M.M. Suhoski, A. Varela-Rohena, T.N. Golovina, R.G. Carroll, J.L. Riley, and C.H. June. 2010. The inducible costimulator (ICOS) is critical for the development of human T(H)17 cells. *Sci. Transl. Med.* 2:55ra78. https://doi.org/10.1126/scitranslmed.3000448

Reilly, R.T., M.B. Gottlieb, A.M. Ercolini, J.P. Machiels, C.E. Kane, F.I. Okoye, W.J. Muller, K.H. Dixon, and E.M. Jaffee. 2000. HER-2/neu is a tumor rejection target in tolerized HER-2/neu transgenic mice. *Cancer Res.* 60:3569–3576.

Sen, T., B.L. Rodriguez, L. Chen, C.M.D. Corte, N. Morikawa, J. Fujimoto, S. Cristea, T. Nguyen, L. Diao, L. Li, et al. 2019. Targeting DNA damage response promotes antitumor immunity through STING-mediated T-cell activation in small cell lung cancer. *Cancer Discov.* 9:646–661. https://doi.org/10.1158/2159-8290.CD-18-1020

Slaney, C.Y., B. von Scheidt, A.J. Davenport, P.A. Beavis, J.A. Westwood, S. Mardiana, D.C. Tscharke, S. Ellis, H.M. Prince, J.A. Trapani, et al. 2017. Dual-specific chimeric antigen receptor T cells and an indirect vaccine eradicate a variety of large solid tumors in an immunocompetent, self-antigen setting. *Clin. Cancer Res.* 23:2478–2490. https://doi.org/10.1158/1078-0432.CCR-16-1860

Staedtke, V., R.Y. Bai, K. Kim, M. Darvas, M.L. Davila, G.J. Riggins, P.B. Rothman, N. Papadopoulos, K.W. Kinzler, B. Vogelstein, and S. Zhou. 2018. Disruption of a self-amplifying catecholamine loop reduces cytokine release syndrome. *Nature.* 564:273–277. https://doi.org/10.1038/s41586-018-0774-y

Sterner, R.M., R. Sakemura, M.J. Cox, N. Yang, R.H. Khadka, C.L. Forsman, M.J. Hansen, F. Jin, K. Ayasoufi, M. Hefazi, et al. 2019. GM-CSF inhibition reduces cytokine release syndrome and neuroinflammation but enhances CAR-T cell function in xenografts. *Blood.* 133:697–709. https://doi.org/10.1182/blood-2018-10-881722

Tchou, J., Y. Zhao, B.L. Levine, P.J. Zhang, M.M. Davis, J.J. Melenhorst, I. Kulikovskaya, A.L. Brennan, X. Liu, S.F. Lacey, et al. 2017. Safety and efficacy of intratumoral injections of chimeric antigen receptor (CAR) T cells in metastatic breast cancer. *Cancer Immunol. Res.* 5:1152–1161. https://doi.org/10.1158/2326-6066.CIR-17-0189

Wang, S., R. Song, Z. Wang, Z. Jing, S. Wang, and J. Ma. 2018. S100A8/A9 in Inflammation. *Front. Immunol.* 9:1298. https://doi.org/10.3389/fimmu.2018.01298

Woo, S.-R., M.B. Fuertes, L. Corrales, S. Spranger, M.J. Furdyna, M.Y. Leung, R. Duggan, Y. Wang, G.N. Barber, K.A. Fitzgerald, et al. 2014. STING-dependent cytosolic DNA sensing mediates innate immune recognition of immunogenic tumors. *Immunity.* 41:830–842. https://doi.org/10.1016/j.immuni.2014.10.017

JEM

Supplemental material

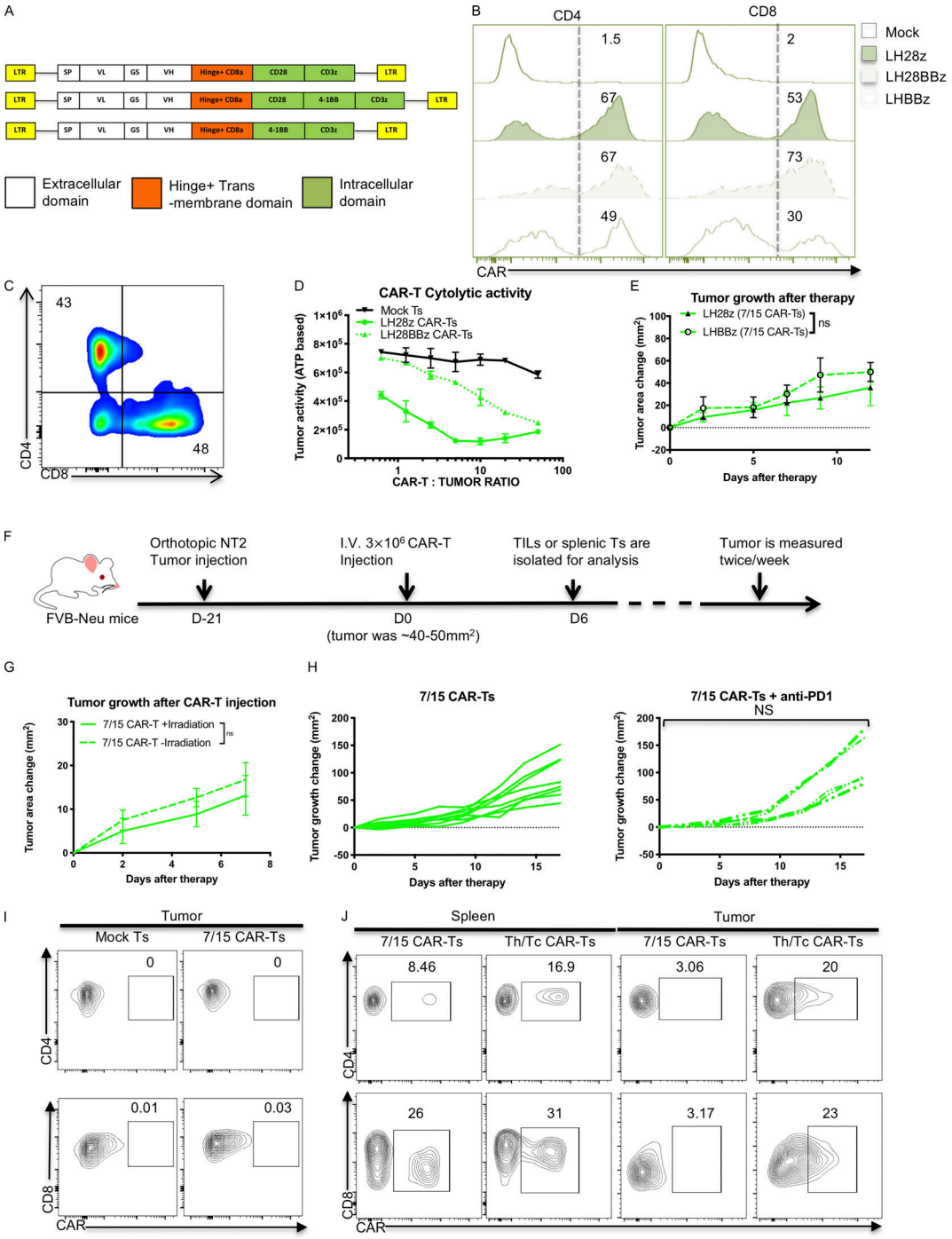

Figure S1. **IL-7/15 cultured CAR T cells fail to control in vitro or in vivo tumor growth control compared with Th/Tc17 CAR T cells. (A)** Schematic of the different CAR cassettes encoding the scFv (7.16.4), hinge and transmembrane domain from CD8 and intracellular domains from CD3ζ, 4-1BB, and/or CD28. **(B)** Expression of CAR T receptor on IL-7/15 cultured LH28BBz or LHBBz CAR T cells compared with LH28z CAR T cells. **(C)** Ratio of $CD4^+$:$CD8^+$ CAR T cells after 6 d of expansion with IL-7 and IL-15. **(D)** NT2 cells were cocultured with different ratios of indicated CAR T cells for 6 h, and tumor cell ATP activity was measured. Tumor ATP level indicating death of tumor cells was characterized at different ratios of mock T cells, LH28z, or LH28BBz CAR T cells. **(E)** Tumor area change was calculated following the administration of IL-7/15 cultured LHBBz or LH28z CAR T cells (3×10^6 CAR T cells intravenously at 1:1 $CD4^+$:$CD8^+$ ratio) into tumor-bearing mice when the tumor size reached 50 mm^2. **(F)** Schematic of the tumor model in which 5×10^4 NT2 tumor cells were injected orthotopically into the mammary fat pad at day −21. Mice received 3×10^6 CAR T cells intravenously at 1:1 $CD4^+$:$CD8^+$ ratio at day 0 when the tumor size reached 50 mm^2. **(G)** Tumor area change was calculated following injection of 7/15 CAR T before lymphopenia induced by 5 Gy total body irradiation. **(H)** Tumor area change was calculated following the administration of anti–PD-1 (200 µg/mouse) twice a week following 7/15 CAR T injection. **(I)** Representative flow cytometry histograms show detection of CAR T cells within the tumor 5 d after 7/15 CAR T infusion. **(J)** Representative flow plots showing detection of CAR T cells within the tumor or spleen 5 d after 7/15 CAR T or Th/Tc17 CAR T infusion. Data are shown as mean ± SD; ns, not significant; significance was determined by Student's *t* test or two-way ANOVA. Mouse studies used a minimum of five mice per group and represent at least two independent experiments. Data were shown as either representative batch or pooled.

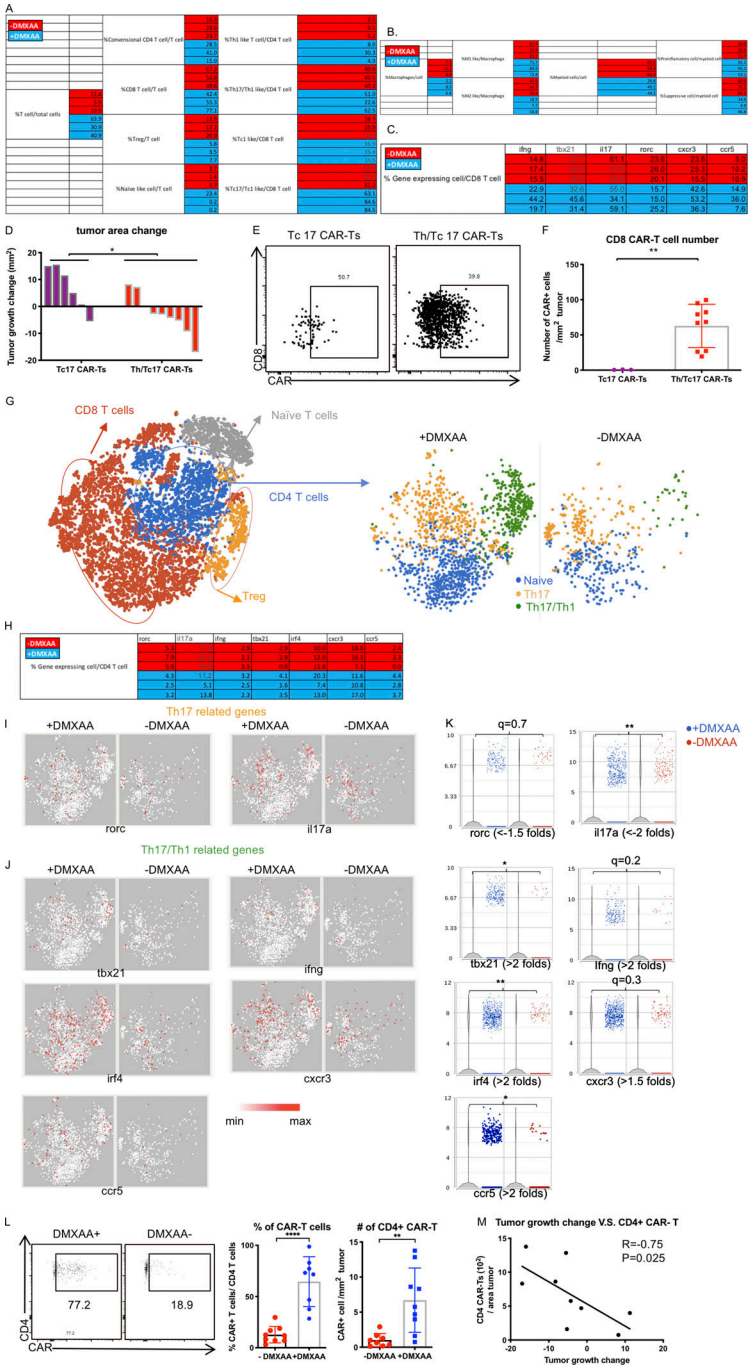

Figure S2. **Th17 CAR T cells are indispensable for DMXAA therapeutic efficacy, which enhances the number and cytotoxicity of Th17 CAR T cells in the TME. (A and B)** Tables for the percentage of T cell subsets (A) and macrophage and myeloid cell subsets (B) calculated from scRNA-seq data. **(C)** Table for the percentage of $CD8^+$ T cells expressing indicated genes calculated from scRNA-seq data. **(D–F)** Assessment of CAR expression on tumor-infiltrating T cells isolated 7 d after therapy by flow cytometry. **(D)** Determination of change in tumor area 7 d after injection of Tc17 or Th/Tc17 CAR T cells. **(E)** Assessment of intratumoral $CD8^+$ CAR T cells was performed 7 d after therapy. **(F)** Absolute number of $CD8^+$ CAR T cells/mm^2 tumor 7 d after therapy. Data in G–M data were derived from the characterization of T cells expressing CD4 from scRNA-seq result. **(G)** $CD4^+$ T cells were subdivided based on absence of *Cd44* (naive T cells), expression of *Cd4* and *Cd44* (activated CD4 T cells), *Cd4* and *Foxp3* (T reg cells). $CD4^+$ T cells were compared between the +DMXAA and −DMXAA treatment groups, and each subpopulation was examined further as described below. **(H)** Table for the percentage of $CD4^+$ T cells expressing the indicated genes from the scRNA-seq data. **(I)** t-SNE plot of $CD4^+$ T cells for Th17-related genes. **(J)** t-SNE plot of $CD4^+$ T cells for Th17/Th1-related genes. **(K)** Violin plot shows the distribution and change of indicated gene expression in B and C. **(L)** Validation of single-cell data using flow cytometry to detect $CD4^+$ CAR T cells. **(M)** Analysis of the correlation between tumor growth change and absolute cell number of CAR-expressing CD4 T cells/cm^2 tumor. Data (excluding scRNA-seq) represent one of two independent experiments ($n \geq 5$ mice per group). Single-cell sequencing data represent three mice/treatment group, with statistical significance determined by differential GSA with the Partek flow workstation. *, $q < 0.05$; **, $q < 0.01$, in the change of gene expression level. Fold change is +DMXAA versus −DMXAA. For percentage/number change, please refer to Fig. S2 H. Flow cytometry data were pooled from two independent experiments and shown as mean ± SD. Statistics analysis for cytometric analysis is determined by Student's *t* test; *, $P < 0.05$; **, $P < 0.01$; ****, $P < 0.0001$.

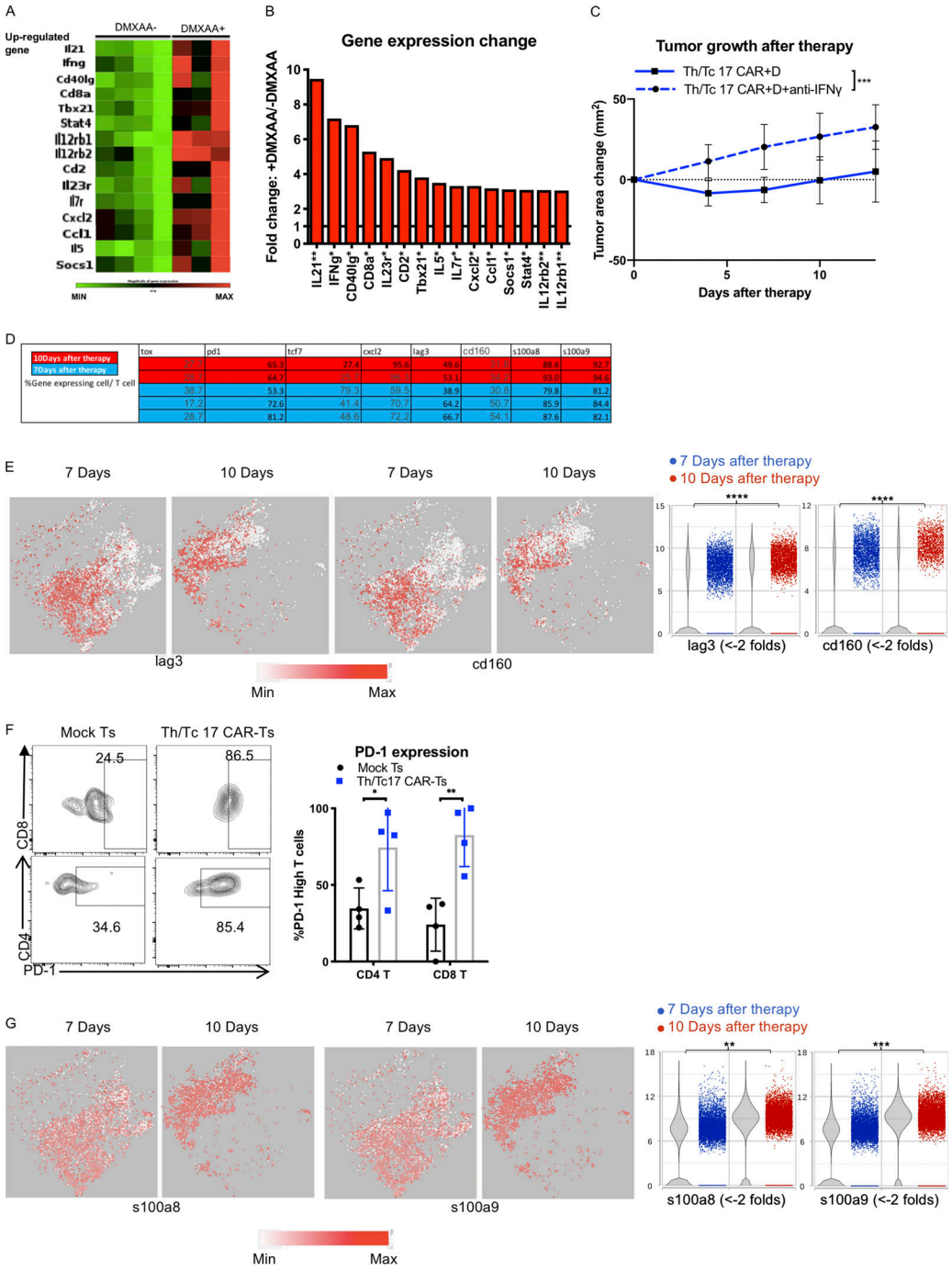

Figure S3. **DMXAA treatment enhances IFN-γ–dependent antitumor function of Th/Tc17 CAR T cells, but T cell exhaustion limits the cumulative beneficial effect of DMXAA on Th/Tc17 CAR T therapy.** Mice received Th/Tc17 CAR T cells in the presence or absence of DMXAA therapy. 7 d later, RNA from tumors was isolated and analyzed by microarray for Th17/Th1 response. **(A)** Heatmap depicts genes where fold-change was significant, with a threefold increase. Each column represents an individual mouse. **(B)** Quantification of significant changes ($P < 0.05$) in TME for Th17 or Th1 response following DMXAA treatment. **(C)** Mice were treated i.p. with anti–IFN-γ (250 µg/mouse) twice a week after Th/Tc17 CAR T therapy. Significance was determined by Student's *t* test or two-way ANOVA. Studies involved at least four mice per independent experiment. Data from C represent two independent experiments with four mice per group. **(D–G)** T cell cluster selected based on expression of *Cd3e* by unsupervised clustering of tumor-infiltrating immune cells from 7 and 10 d after Th/Tc17 CAR + D therapy. **(D)** Table shows the percentage of T cells expressing the indicated genes calculated from scRNA-seq data. **(E)** t-SNE plot (left) and violin plot (right) of T cells for genes associated with T cell exhaustion. **(F)** Validation of PD-1 expression using flow-based method to detect high levels of PD-1 expression on T cells from mice receiving Th/Tc17 CAR T or mock T cell therapy. Representative flow cytometry histograms (left); percentage of CAR T (right) within the CD4 or CD8 T cell group ($n = 4$/group). **(G)** t-SNE plot (left) and violin plot (right) of T cells for genes associated with T cell apoptosis. Data (excluding scRNA-seq) represent one of two independent experiments ($n \geq 5$ mice per group). Single-cell sequencing data represent two to three mice/treatment group. Statistical significance was determined by differential GSA with the Partek flow workstation. *, $q < 0.05$; **, $q < 0.01$; ***, $q < 0.001$; ****, $q < 0.0001$ in the change of gene expression level. Fold change is 7 versus 10 d. For percentage/number change, please refer to Fig. S3 D. Flow cytometric analysis is shown as mean ± SD. Statistics analysis for cytometric analysis was determined by Student's *t* test; *, $P < 0.05$; **, $P < 0.01$; ***, $P < 0.001$; ****, $P < 0.0001$.

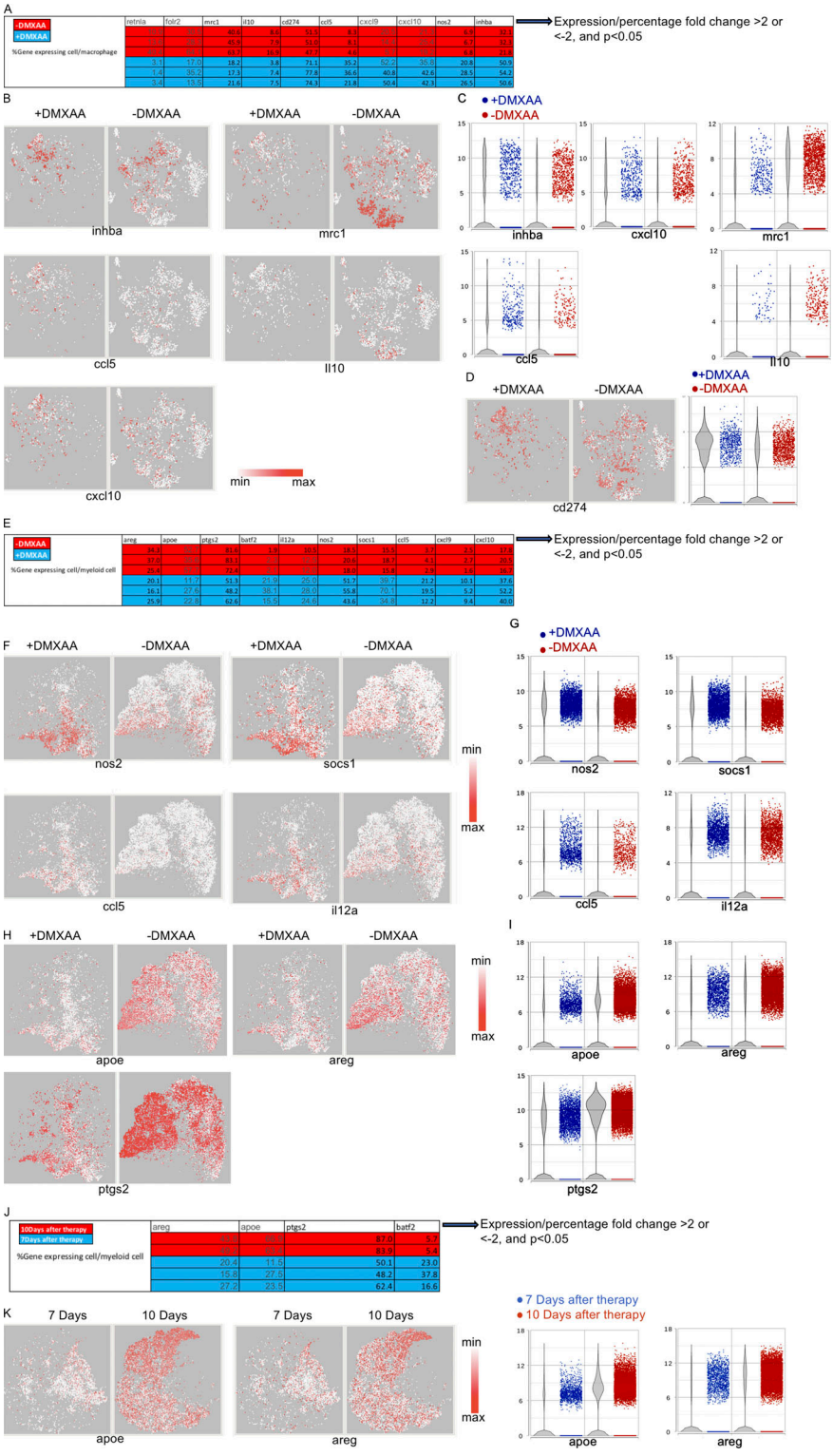

Figure S4. **M2 macrophages and myeloid cells are reduced upon DMXAA treatment, but later replaced by suppressive myeloid cells.** Macrophages and myeloid cells from day 7 are selected as in Fig. 3 F. **(A)** Table showing the percentage of macrophages expressing the indicated genes calculated from scRNA-seq data. **(B)** t-SNE plot on M1-like (left) and M2-like (right) related genes. **(C)** Violin plot shows the distribution and change of indicated gene expression in B. **(D)** t-SNE and violin plot of *cd274* (PD-L1). **(E)** Table showing the percentage of myeloid cells expressing the indicated gene calculated from scRNA-seq data. **(F)** t-SNE plot on genes expressed in iMCs. **(G)** Violin plot shows the distribution and change of indicated gene expression in F. **(H)** t-SNE plot of genes expressed in myeloid-like suppressor cells. **(I)** Violin plot shows the distribution and change of indicated gene expression in H. Myeloid cells from days 7 and 10 are selected as in Fig. 3 J. **(J)** Table showing the percentage of myeloid cells expressing the indicated genes calculated from scRNA-seq data. **(K)** t-SNE plot (left) and violin plot (right) of myeloid cells for genes associated with myeloid-like suppressor cells. Single-cell sequencing data represent two to three mice/treatment group.

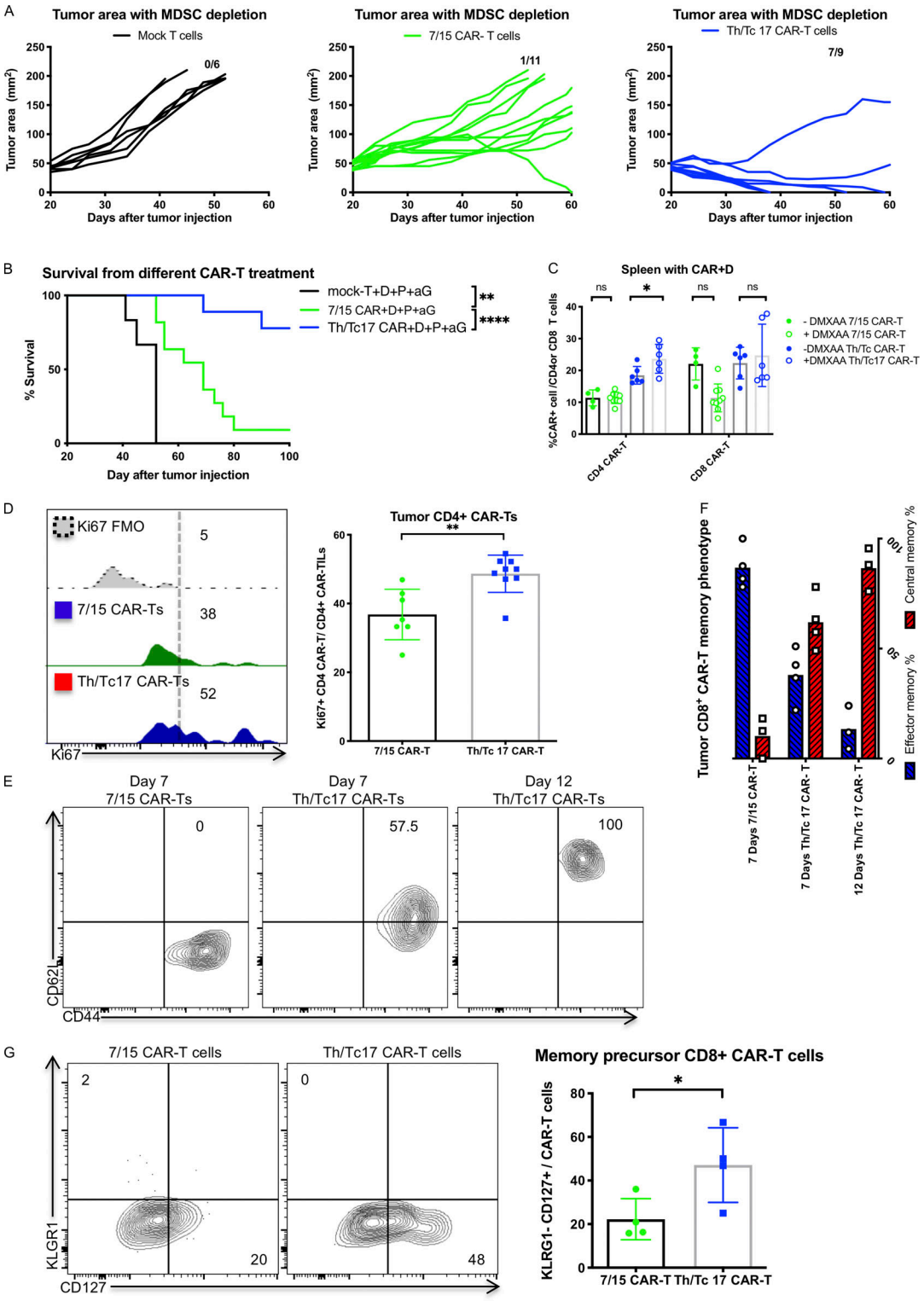

Figure S5. **Th/Tc17 cells function better than IL-7/15 CAR T cells when combined with a STING agonist, anti–PD-1, and anti–GR-1 mAb therapy.** Mice were treated with anti–GR-1, anti–PD-1, DMXAA, and Th/Tc17 CAR T cells, 7/15 CAR T cells, or mock T cells as described in Fig. S5. **(A)** Tumor growth in individual mice receiving therapy. **(B)** Kaplan–Meier survival curve. **(C)** Summary of CAR T cell accumulation in the spleen. **(D–G)** Mice received 7/15 CAR + D + aP or Th/Tc17 CAR + D + aP treatment. T cells were isolated from the tumor 7 d after therapy and characterized by flow cytometry. **(D)** Representative plot (left) and summary graph (right) of Ki67 expression from CD4⁺ CAR T cells with six to nine mice per group. **(E and F)** Assessment of the memory phenotype of CD8⁺ CAR T cells from the tumor at 7 or 12 d after 7/15 CAR + D + aP or Th/Tc17 CAR + D + aP treatment. **(G)** Comparison of memory precursor effector cells of CD8⁺ CAR T cells within the tumor 7 d after 7/15 CAR + D + aP or Th/Tc17 CAR + D + aP treatment. Data shown as mean ± SD; ns, not significant; *, P < 0.05; **, P < 0.01; ***, P < 0.001; ****, P < 0.0001, significance was determined by Student's *t* test or log-rank Mantel–Cox test comparing survival. Mouse studies used a minimum of five mice per group and represent at least two independent experiments where data are shown as either representative or pooled.